A Hyperbolic Two-Fluid Model for Compressible Flows with Arbitrary Material-Density Ratios

Rodney Fox, Frédérique Laurent, Aymeric Vié

A Hyperbolic Two-Fluid Model for Compressible Flows with Arbitrary Material-Density Ratios

Rodney O. Fox[1,2,4], Frédérique Laurent[3,4], Aymeric Vié[3,4]

[1]Department of Chemical and Biological Engineering, 618 Bissell Road, Iowa State University, Ames, IA 50011-1098, USA

[2]Center for Multiphase Flow Research and Education, 537 Bissell Road, Iowa State University, Ames, IA 50011-1096, USA

[3]Laboratoire EM2C UPR 288, CNRS, CentraleSupélec, Université Paris-Saclay, 3, rue Joliot-Curie 91192 Gif-sur-Yvette cedex France

[4]Fédération de Mathématiques de CentraleSupélec, CNRS, 3, rue Joliot-Curie 91192 Gif-sur-Yvette cedex France

(Received xx; revised xx; accepted xx)

A hyperbolic two-fluid model for gas–particle flow derived using the Boltzmann–Enskog kinetic theory is generalized to include added mass. In place of the virtual-mass force, to guarantee indifference to an accelerating frame of reference, the added mass is included in the mass, momentum and energy balances for the particle phase, augmented to include the portion of the particle wake moving with the particle velocity. The resulting compressible two-fluid model contains seven balance equations (mass, momentum, and energy for each phase, plus added mass) and employs a stiffened-gas model for the equation of state for the fluid. Using Sturm's theorem, the model is shown to be globally hyperbolic for arbitrary ratios of the material densities $Z = \rho_f/\rho_p$. An eight-equation extension to include the pseudo-turbulent kinetic energy (PTKE) in the fluid phase is also proposed; however, PTKE has no effect on hyperbolicity. In addition to the added mass, the key physics needed to ensure hyperbolicity for arbitrary Z is a fluid-mediated contribution to the particle-phase pressure tensor that is taken to be proportional to the volume fraction of the added mass. A numerical solver for hyperbolic equations is developed for the 1-D model, and numerical examples are employed to illustrate the behaviour of solutions to Riemann problems for different material-density ratios. The relation between the proposed two-fluid model and prior work on effective-field models is discussed, as well as possible extensions to include viscous stresses and the formulation of the model in the limit of an incompressible continuous phase.

Key words: compressible flow, hyperbolic two-fluid model, disperse multiphase flow, material-density ratio

1. Introduction

The difficulties in developing hyperbolic two-fluid models for disperse multiphase flows has been reviewed by Lhuillier *et al.* (2013). Many of the models that have been proposed in the literature suffer from being mathematically ill-posed (see Drew & Passman 1998; Vazquez-Gonzalez *et al.* 2016, for other discussions of this topic), most notably when the

Archimedes force is included. Mathematically, well-posedness of non-linear multiphase flow models implies hyperbolicity of the underlying Cauchy problem (Métivier 2005). In practice, numerical simulations with non-hyperbolic two-fluid models diverge under grid refinement due to the complex eigenvalues in the continuum limit (see, e.g., Ndjinga 2007; Kumbaro & Ndjinga 2011). To solve this problem, *ad hoc* correction terms have been added to make the models well-posed (see, e.g., Panicker *et al.* 2018). In particular, some authors have resorted to neglecting the Archimedes force (see, e.g., Hank *et al.* 2011), which is the root cause of non-hyperbolicity. For bubbly flows the Archimedes force is of critical importance when buoyancy effects are present.

Starting from a kinetic-theory description, Fox (2019) developed a hyperbolic two-fluid model for gas–particle flows that neglects added-mass effects (as well as inelastic collisions and viscous effects). The model equations were derived starting from the Boltzmann–Enskog kinetic theory for a binary hard-sphere mixture. A closure for the particle-pair distribution functions was introduced to account for the Archimedes force in the limit where one particle diameter is much smaller than the other. However, because the closure for the particle-pair distribution function only accounts for mean gradients, it cannot capture the higher-order correlations needed for added mass. The system of velocity moment equations was truncated at second order, and the unclosed collisional source terms were closed using an isotropic Gaussian (Maxwellian) distribution (Levermore & Morokoff 1996; Vié *et al.* 2015). Then, by employing Sturm's theorem (Sturm 1829), it was demonstrated that the resulting two-fluid model is hyperbolic for physically realistic values of the model parameters. In comparison to other two-fluid models, novel contributions to the pressure tensor and energy flux (which appear in closed form) arise and play a key role in ensuring hyperbolicity when fluid and particle material densities satisfy $\rho_f \ll \rho_p$. Here, we employ the same model formulation, extended to account for the added mass from particle wakes and pseudo-turbulence, to compressible fluid–particle flows with a slip velocity due, e.g., to buoyancy.

Our treatment of added mass is similar to Cook & Harlow (1984) (see appendix A for more details), but generalized to a compressible fluid and a non-constant added-mass function. The latter is required to handle flows wherein the particle-phase volume fraction varies significantly. In our model and in the model of Cook & Harlow (1984), mathematical objectivity is ensured, unlike in other formulations (e.g., Drew *et al.* 1979; Massoudi 2002). In the context of kinetic theory, the approach of Cook & Harlow (1984) where the added mass moves with the particle velocity allows us to simply redefine the particle properties without changing the basic form of the kinetic equation governing the velocity distribution function (Fox 2019). Nonetheless, because the fluid in the particle wake is not fixed, but exchanges with the bulk fluid, mass transfer must be included in the kinetic equation to model the convective mass-transfer process. Here, a simple model is employed that depends on a mass-exchange function S_a. (See figure 1 for details.) Because the mass-transfer model involves neither spatial nor temporal derivatives, its form does not affect the hyperbolicity of the two-fluid model.

From a kinetic-theory perspective, the added mass of fluid on a particle can be accounted for by defining a particle's volume and mass to include the fluid moving with the particle (Marchisio & Fox 2013), i.e., the fluid in the particle wake (Moore & Balachandar 2019). The total particle mass m_p is then employed in the kinetic-theory expressions for the velocity moments. This procedure introduces two volume fractions, namely α_p and $\alpha_p^\star = \alpha_p + \alpha_a$. The former is the usual volume fraction of the particle phase, while the latter includes the volume of the fluid moving with the particles. Naturally $\alpha_p^\star \geqslant \alpha_p$ and the corresponding fluid-phase volume fractions are $\alpha_f^\star = 1 - \alpha_p^\star$ and $\alpha_f = 1 - \alpha_p$, respectively. A similar decomposition of the fluid-phase variables is used by

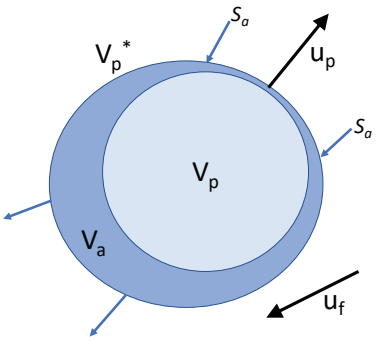

FIGURE 1. Schematic of a particle with its added volume of fluid (i.e., the wake of the particle). The fluid in the wake exchanges mass with the external fluid at a net rate determined by S_a. The total particle volume, moving with velocity $\boldsymbol{u}_p$, is $V_p^\star$ with sub-volume V_p having material density ρ_p and added volume V_a having material density ρ_f. The external fluid with material density ρ_f and moving with velocity $\boldsymbol{u}_f$, has volume $V_f^\star = V - V_p^\star$. The mass of the particle is $m_p = \rho_p V_p + \rho_f V_a$. In terms of the volume fractions, $m_p = (\rho_p \alpha_p + \rho_f \alpha_a)V = \rho_e \alpha_p^\star V$ where ρ_e is the effective density of the particle with its added mass and $\alpha_p^\star = \alpha_p + \alpha_a$. Thus, the added volume of fluid moving with the particle velocity is $\alpha_a V$, and the added mass is $\rho_f \alpha_a V$. The added-volume fraction must satisfy $0 \leqslant \alpha_a \leqslant \alpha_f$ so it is convenient to define an added-mass function c_m by $\alpha_a = c_m \alpha_p \alpha_f$. As the added volume is usually associated with particle wakes, c_m can depend on the particle Reynolds number Re_p, the particle-phase volume fraction, and other dimensionless parameters needed to describe the flow. In the limit $\alpha_p \to 1$, all of the fluid can be assumed to move with the particle so that $c_m \to 1$; however, this is not required for hyperbolicity.

Osnes *et al.* (2019) to define a modified slip velocity ($\boldsymbol{u}_{free} = \alpha_f \boldsymbol{u}_{fp}/\alpha_f^\star$) in supersonic gas–particle flows. Using arguments similar to those of Risso (2018) for bubbly flows, these authors also reported that the pseudo-turbulence in the stream-wise direction is well approximated by $\alpha_a u_{fp}^2/\alpha_f^\star$, and for fixed α_p show that α_a decreases with increasing Re_p (Osnes *et al.* 2020).

For the analysis of hyperbolicity, it is convenient to introduce an added-mass function c_m defined such that $\alpha_a = c_m \alpha_p \alpha_f$. In principle, c_m can be a function of the slip velocity between the two phases (i.e., of the particle Reynolds number $Re_p = \rho_f d_p u_{fp}/\mu_f$ where d_p is the particle diameter and μ_f is fluid viscosity), the density ratio $Z = \rho_p/\rho_f$, and the volume fraction α_p (Zuber 1964; Sangani *et al.* 1991; Zhang & Prosperetti 1994). However, in the dilute limit, Odar & Hamilton (1964) found experimentally that c_m depends only on the acceleration number $Ac = u_{fp}^2/(ad_p)$ where a is the magnitude of the particle acceleration, which we approximation below using the drag force. Unless $c_m = 0$, the phase velocities found from the kinetic-theory derivation will not be equal to those found from volume averaging unless added mass is accounted for in the latter. Nevertheless, the kinetic-theory derivation leads to conservation laws in the form of hyperbolic equations. This has advantages over a formulation where the virtual mass is treated as an interphase force when solving the two-fluid model numerically.

Finally, because the added mass can vary from location to location in the flow, mass transfer between the bulk fluid and the added-mass fluid (i.e., the particle wake) must be accounted for in the model. This is done by introducing an added-mass exchange rate S_a. The exchange of mass between the bulk fluid and added mass also induces an exchange of momentum and kinetic energy, which depends on the direction of the mass exchange. The bulk-fluid momentum is $\rho_f \alpha_f^\star \boldsymbol{u}_f$, while that of the added-mass fluid is

$\rho_f \alpha_a \boldsymbol{u}_p$. Concerning the total energy, for the particle phase it is defined by

$$\rho_e \alpha_p^\star E_p = \rho_e \alpha_p^\star \left(\frac{\Theta_p}{\gamma_p - 1} + \frac{1}{2} u_p^2 \right), \tag{1.1}$$

where $\gamma_p = 5/3$ for hard spheres, Θ_p is the granular temperature, and $\rho_e \alpha_p^\star = \rho_p \alpha_p + \rho_f \alpha_a$ defines ρ_e. For simplicity, in (1.1) the internal energy associated with the solid phase *and the added mass* is neglected. Otherwise, an additional scalar transport equation would be required, which does not change the hyperbolicity of the system (Houim & Oran 2016). For the bulk fluid, the total energy is defined by

$$\rho_f \alpha_f^\star E_f = \rho_f \alpha_f^\star \left(\frac{\Theta_f}{\gamma_f - 1} + \frac{1}{2} u_f^2 + k_f \right) \tag{1.2}$$

where γ_f is the fluid specific heat ratio, Θ_f is the fluid temperature and k_f is the pseudo-turbulent kinetic energy (PTKE). In the two-fluid model, the momentum-exchange contribution is equal to $S_a \boldsymbol{u}_f$ or $S_a \boldsymbol{u}_p$, and the energy-exchange contribution to $S_a(\frac{1}{2} u_f^2 + k_f)$ or $S_a E_p$, depending on the sign of S_a. The asymmetry in the energy exchange from the bulk fluid to the particle wake results from neglecting the internal energy in (1.1). In the compressible two-fluid model, (1.1) and (1.2) are used to find the temperatures Θ_p and Θ_f given the total energies E_p and E_f, respectively. In the stiffened-gas model used for the fluid, Θ_f must be initialized such that the fluid pressure p_f is positive.

2. Two-fluid model for compressible flows

2.1. *Governing equations*

The governing equations for mono-disperse particles in a compressible fluid with added mass, but neglecting PTKE, are given in table 1. If PTKE is taken into account (Shallcross *et al.* 2020), the model has the form given in table 2. We should point out that in the balance equation for k_f the part of the source term D_{PT} due to drag is $K u_{fp}^2$, which is the same as the correlated part of the source term for total energy D_E. Physically, this implies that viscous losses are ignored during the exchange process such that drag transfers energy to k_f from the particle phase, which is subsequently dissipated to uncorrelated energy by ε_{PT}. The accuracy of this assumption is likely to depend on the particle Reynolds number, i.e. it will be more accurate for high Re_p where the particle wakes are turbulent. In practice, this difference can be accounted for by multiplying $K u_{fp}^2$ in D_{PT} (but not in D_E) by a damping factor dependent on Re_p. Doing so, it may be possible to reduce the Mach-number dependence of C_f observed in Shallcross *et al.* (2020).

In prior work (Fox 2019), it has been demonstrated that for an ideal gas ($\gamma_f = 5/3$) with material densities such that $\rho_p \gg \rho_f$ and $\alpha_a = 0$ the two-fluid model in table 1 is hyperbolic for physically relevant values of the parameters. In this work, we mainly consider the opposite case with $\rho_p \ll \rho_f$ where the fluid phase is described by the stiffened-gas model (Harlow & Amsden 1971; Saurel & Abgrall 1999). For a pure fluid, the latter gives an equation of state of the form $p_f = \rho_f \Theta_f - p_f^o$ where the constant p_f^o is used to set the speed of sound in the fluid phase. For example, water can be simulated with $p_f^o \approx 2225$ MPa. The fluid temperature Θ_f ($\mathrm{m}^2/\mathrm{s}^2$) is found from the fluid energy E_f as shown in table 1, and must be large enough that $p_f > 0$. In this work, we will use a stiffened-gas model of the form

$$p_f = \rho_f \Theta_f - \gamma_f(\gamma_f - 1) p_f^o \frac{\alpha_f}{\alpha_f^\star}. \tag{2.1}$$

$$\partial_t(\rho_p\alpha_p) + \partial_{\mathbf{x}}\cdot(\rho_p\alpha_p\boldsymbol{u}_p) = 0$$
$$\partial_t(\rho_e\alpha_p^\star) + \partial_{\mathbf{x}}\cdot(\rho_e\alpha_p^\star\boldsymbol{u}_p) = S_a$$
$$\partial_t(\rho_f\alpha_f^\star) + \partial_{\mathbf{x}}\cdot(\rho_f\alpha_f^\star\boldsymbol{u}_f) = -S_a$$

$$\partial_t(\rho_e\alpha_p^\star\boldsymbol{u}_p) + \partial_{\mathbf{x}}\cdot(\rho_e\alpha_p^\star\boldsymbol{u}_p\boldsymbol{u}_p + p_p\boldsymbol{I}) = K\boldsymbol{u}_{fp} - \partial_{\mathbf{x}}\cdot(\alpha_a\boldsymbol{P}_{fp}^a) - \alpha_p^\star\partial_{\mathbf{x}}p_f + \boldsymbol{S}_{fp} - \boldsymbol{F}_{pf} + \rho_e\alpha_p^\star\boldsymbol{g}$$

$$\partial_t(\rho_f\alpha_f^\star\boldsymbol{u}_f) + \partial_{\mathbf{x}}\cdot(\rho_f\alpha_f^\star\boldsymbol{u}_f\boldsymbol{u}_f + p_f\boldsymbol{I} + \alpha_p^\star\rho_f\boldsymbol{R}) = K\boldsymbol{u}_{pf} + \partial_{\mathbf{x}}\cdot(\alpha_a\boldsymbol{P}_{fp}^a) + \alpha_p^\star\partial_{\mathbf{x}}p_f - \boldsymbol{S}_{fp} + \boldsymbol{F}_{pf} + \rho_f\alpha_f^\star\boldsymbol{g}$$

$$\partial_t(\rho_e\alpha_p^\star E_p) + \partial_{\mathbf{x}}\cdot(\rho_e\alpha_p^\star E_p\boldsymbol{u}_p + p_p\boldsymbol{u}_p) = -D_E - \boldsymbol{u}_p\cdot(\partial_{\mathbf{x}}\cdot\alpha_a\boldsymbol{P}_{fp}^a) - \alpha_p^\star\boldsymbol{u}_p\cdot\partial_{\mathbf{x}}p_f + S_E - D_{pf} + \rho_e\alpha_p^\star\boldsymbol{u}_p\cdot\boldsymbol{g}$$

$$\partial_t(\rho_f\alpha_f^\star E_f) + \partial_{\mathbf{x}}\cdot(\rho_f\alpha_f^\star E_f\boldsymbol{u}_f + \alpha_f^\star p_f\boldsymbol{u}_f + \alpha_p^\star p_f\boldsymbol{u}_p + \alpha_p^\star\rho_f\boldsymbol{R}\cdot\boldsymbol{u}_p + \boldsymbol{r}) = D_E + \boldsymbol{u}_p\cdot(\partial_{\mathbf{x}}\cdot\alpha_a\boldsymbol{P}_{fp}^a) + \alpha_p^\star\boldsymbol{u}_p\cdot\partial_{\mathbf{x}}p_f - S_E + D_{pf} + \rho_f\alpha_f^\star\boldsymbol{u}_f\cdot\boldsymbol{g}$$

where ρ_p is constant,

$$\alpha_p^\star = \alpha_p + \alpha_a \qquad \rho_e = \frac{\rho_p\alpha_p + \rho_f\alpha_a}{\alpha_p + \alpha_a} \qquad \alpha_f^\star = 1 - \alpha_p^\star \qquad \alpha_f = 1 - \alpha_p$$

and the added-mass source terms are

$$S_a = \frac{1}{\tau_a}\rho_f\alpha_f\alpha_p(c_m^\star - c_m) \qquad \boldsymbol{S}_{fp} = \max(S_a,0)\boldsymbol{u}_f + \min(S_a,0)\boldsymbol{u}_p$$

$$\tau_a = \frac{4d_p^2\alpha_f^\star}{3\nu_f C_D Re_p\alpha_f} \qquad S_E = \max(S_a,0)\frac{1}{2}u_f^2 + \min(S_a,0)E_p$$

The other variables are defined as follows:

$$\boldsymbol{u}_{fp} = -\boldsymbol{u}_{pf} = \boldsymbol{u}_f - \boldsymbol{u}_p \qquad p_f = \rho_f\Theta_f - \gamma_f(\gamma_f-1)p_f^o\frac{\alpha_f}{\alpha_f^\star} \qquad p_p = \rho_e\alpha_p^\star\Theta_p(1+4\alpha_p^\star g_0)$$

$$\boldsymbol{R} = \left(\Theta_p + \frac{1}{3\gamma_p}u_{fp}^2\right)\boldsymbol{I} + \frac{2}{3\gamma_p}\boldsymbol{u}_{fp}\otimes\boldsymbol{u}_{fp} \qquad \boldsymbol{P}_{fp}^a = \frac{2\rho_f}{3\gamma_p}\left(\frac{1}{2}u_{fp}^2\boldsymbol{I} + \boldsymbol{u}_{fp}\otimes\boldsymbol{u}_{fp}\right)(1+4\alpha_p^\star g_0)$$

$$\boldsymbol{F}_{pf} = \alpha_p^\star\boldsymbol{R}\cdot\partial_{\mathbf{x}}\rho_f + (\gamma_p-1)\rho_f\alpha_p^\star\left(tr(\boldsymbol{\Gamma})\boldsymbol{I} + \frac{2}{\gamma_p}\boldsymbol{S}\right)\cdot\boldsymbol{u}_{fp} \qquad \boldsymbol{r} = 2\rho_f\alpha_p^\star\Theta_p\boldsymbol{u}_{pf}$$

$$D_{pf} = \boldsymbol{u}_p\cdot\boldsymbol{F}_{pf} + 2\alpha_p^\star\Theta_p\left[\boldsymbol{u}_{pf}\cdot\partial_{\mathbf{x}}\rho_f - \rho_f tr(\boldsymbol{\Gamma})\right] \qquad D_E = K\left(3\Theta_p + \boldsymbol{u}_p\cdot\boldsymbol{u}_{pf}\right)$$

$$\Theta_f = (\gamma_f-1)\left(E_f - \frac{1}{2}u_f^2\right) \qquad \Theta_p = (\gamma_p-1)\left(E_p - \frac{1}{2}u_p^2\right) \qquad g_0 = \frac{1+\alpha_f}{2\alpha_f^3}$$

$$K = \frac{3\rho_p\alpha_p^\star C_D Re_p}{4\tau_p} \quad \tau_p = \frac{\rho_p d_p^2}{\mu_f} \qquad \boldsymbol{S} = \boldsymbol{\Gamma} - \frac{1}{3}tr(\boldsymbol{\Gamma})\boldsymbol{I} \qquad \boldsymbol{\Gamma} = \frac{1}{2}\left[(\partial_{\mathbf{x}}\otimes\boldsymbol{u}_f) + (\partial_{\mathbf{x}}\otimes\boldsymbol{u}_f)^t\right]$$

TABLE 1. Compressible two-fluid model for particles in a fluid modelled as a stiffened gas. Typical values of the specific heat ratios are $\gamma_f = 29/4$ and $\gamma_p = 5/3$, and for the stiffened-gas constant $p_f^o = 10^8$ kg/m·s^2. C_D is the drag coefficient that depends on the particle Reynolds number Re_p, fluid Mach number, and volume fraction; and $\boldsymbol{g}$ is gravity. The default added-mass function is $c_m^\star = \frac{1}{2}\min(1+2\alpha_p, 2)$.

The actual value of p_f^o is not important as long as the speed of sound is much larger than the other characteristic velocities (or eigenvalues) of the system. The factor $\alpha_f/\alpha_f^\star$ has been added to handle the limiting case where $\alpha_f \to 0$ (i.e. densely packed particles), for which this ratio diverges. Other forms of the stiffened-gas model are possible, and the factor is not needed for more dilute systems where the disperse-phase eigenvalues remain well separated from those of the fluid phase. For the disperse (i.e., particle) phase, the radial distribution function g_0 controls the speed of sound as α_f approaches zero. For example, if g_0 is replaced with unity, the particle-phase speed of sound is weakly dependent on α_p. Here, to analysis the hyperbolicity of the two-fluid model, we use a form for g_0 applicable to non-deformable spheres, but other forms can be used as long as $1 \leqslant g_0$. Furthermore, replacing $\alpha_f/\alpha_f^\star$ with g_0 in (2.1) will not change the conclusions drawn in §3 concerning the hyperbolicity of the two-fluid models.

The kinetic-theory model derived in Fox (2019) made specific assumptions concerning the two-particle distribution function that may be inaccurate for non-ideal gases and liquids. Specifically, the terms involving $\boldsymbol{R}$ and $\boldsymbol{r}$ in table 1 are exact for hard-sphere collisions (i.e., $\gamma_f = \gamma_p = 5/3$), but their definition in a stiffened gas is less obvious (e.g., should they depend on both γ_f and γ_p?). Thus, in our analysis of the hyperbolicity of the two-fluid model in §3 we also consider a simplified version where these terms are neglected in the fluid phase. Nonetheless, because the particle-phase pressure tensor $\boldsymbol{P}_p$ includes an added-mass contribution involving $\boldsymbol{R}$, one can argue that $\boldsymbol{P}_p$ has its origins in the kinetic-theory description. In fact, in §3 we show that the eigenvalues of the 1-D model are mainly determined by the choice of $\boldsymbol{P}_p$ and p_f, with $\boldsymbol{R}$ and $\boldsymbol{r}$ in the fluid phase only slightly changing the eigenvalues (while making the hyperbolicity analysis more complicated). Thus, from the standpoint of applications to real systems, the simplified model may offer a good compromise between computation cost and model accuracy. However, one would also need to account for inelastic collisions, particle-phase viscosity, as well as other effects (see, e.g., Abbas *et al.* 2010) in most applications, none of which affect the hyperbolicity.

2.2. *Added-mass model*

In addition to the fluid drag with coefficient K, the models in tables 1 and 2 include the buoyancy force, compressibility, lift, and added mass. Compressibility and lift are contained in the exchange force $\boldsymbol{F}_{pf}$ (Fox 2019). The added-mass contribution is treated differently than in most other two-fluid models where balance equations are written for each phase with a virtual-mass force. Instead, here the phases are defined by their velocities $\boldsymbol{u}_p$ and $\boldsymbol{u}_f$, and the added mass moves with the particle velocity $\boldsymbol{u}_p$ (see discussion in Cook & Harlow 1984). For example, the mass per unit volume of the fluid phase moving with velocity $\boldsymbol{u}_f$ is $\rho_f\alpha_f^\star = \rho_f(\alpha_f - \alpha_a)$. Note that

$$\rho_f\alpha_f^\star + \rho_e\alpha_p^\star = \rho_f\alpha_f + \rho_p\alpha_p \tag{2.2}$$

so that the mixture density is independent of α_a. The various volume fractions appearing in the model are related by

$$\alpha_f^\star = \alpha_f - \alpha_a \qquad \alpha_p^\star = \alpha_p + \alpha_a \qquad \alpha_p + \alpha_f = 1. \tag{2.3}$$

Given the conserved variables $(X_1, X_2, X_3) = (\rho_p\alpha_p, \rho_e\alpha_p^\star, \rho_f\alpha_f^\star)$ and the particle density ρ_p, the volume fractions and fluid density are uniquely determined by

$$(\alpha_p, \rho_f, \alpha_a) = \left(\frac{X_1}{\rho_p}, \frac{X_3 + X_2 - X_1}{\alpha_f}, \frac{X_2 - X_1}{\rho_f}\right). \tag{2.4}$$

$$\partial_t(\rho_p\alpha_p) + \partial_{\mathbf{x}}\cdot(\rho_p\alpha_p\boldsymbol{u}_p) = 0$$
$$\partial_t(\rho_e\alpha_p^\star) + \partial_{\mathbf{x}}\cdot(\rho_e\alpha_p^\star\boldsymbol{u}_p) = S_a$$
$$\partial_t(\rho_f\alpha_f^\star) + \partial_{\mathbf{x}}\cdot(\rho_f\alpha_f^\star\boldsymbol{u}_f) = -S_a$$

$$\partial_t(\rho_e\alpha_p^\star\boldsymbol{u}_p) + \partial_{\mathbf{x}}\cdot(\rho_e\alpha_p^\star\boldsymbol{u}_p\boldsymbol{u}_p + p_p\boldsymbol{I}) = K\boldsymbol{u}_{fp} - \partial_{\mathbf{x}}\cdot(\alpha_a\boldsymbol{P}_{fp}^a) - \alpha_p^\star\partial_{\mathbf{x}}\cdot\boldsymbol{P}_f + \boldsymbol{S}_{fp} - \boldsymbol{F}_{pf} + \rho_e\alpha_p^\star\boldsymbol{g}$$

$$\partial_t(\rho_f\alpha_f^\star\boldsymbol{u}_f) + \partial_{\mathbf{x}}\cdot(\rho_f\alpha_f^\star\boldsymbol{u}_f\boldsymbol{u}_f + \boldsymbol{P}_f + \alpha_p^\star\rho_f\boldsymbol{R}) = K\boldsymbol{u}_{pf} + \partial_{\mathbf{x}}\cdot(\alpha_a\boldsymbol{P}_{fp}^a) + \alpha_p^\star\partial_{\mathbf{x}}\cdot\boldsymbol{P}_f - \boldsymbol{S}_{fp} + \boldsymbol{F}_{pf} + \rho_f\alpha_f^\star\boldsymbol{g}$$

$$\partial_t(\rho_e\alpha_p^\star E_p) + \partial_{\mathbf{x}}\cdot(\rho_e\alpha_p^\star E_p\boldsymbol{u}_p + p_p\boldsymbol{u}_p) = -D_E - \boldsymbol{u}_p\cdot(\partial_{\mathbf{x}}\cdot\alpha_a\boldsymbol{P}_{fp}^a) - \alpha_p^\star\boldsymbol{u}_p\cdot(\partial_{\mathbf{x}}\cdot\boldsymbol{P}_f) + S_E - D_{pf} + \rho_e\alpha_p^\star\boldsymbol{u}_p\cdot\boldsymbol{g}$$

$$\partial_t(\rho_f\alpha_f^\star E_f) + \partial_{\mathbf{x}}\cdot(\rho_f\alpha_f^\star E_f\boldsymbol{u}_f + \alpha_f^\star\boldsymbol{P}_f\cdot\boldsymbol{u}_f + \alpha_p^\star\boldsymbol{P}_f\cdot\boldsymbol{u}_p + \alpha_p^\star\rho_f\boldsymbol{R}\cdot\boldsymbol{u}_p + \boldsymbol{r}) = D_E + \boldsymbol{u}_p\cdot(\partial_{\mathbf{x}}\cdot\alpha_a\boldsymbol{P}_{fp}^a) + \alpha_p^\star\boldsymbol{u}_p\cdot(\partial_{\mathbf{x}}\cdot\boldsymbol{P}_f) - S_E + D_{pf} + \rho_f\alpha_f^\star\boldsymbol{u}_f\cdot\boldsymbol{g}$$

$$\partial_t(\rho_f\alpha_f^\star k_f) + \partial_{\mathbf{x}}\cdot(\rho_f\alpha_f^\star k_f\boldsymbol{u}_f) + \rho_f\alpha_f^\star\boldsymbol{R}_f : \partial_{\mathbf{x}}\boldsymbol{u}_f = D_{PT} - \rho_f\alpha_f^\star\varepsilon_{PT}$$

In addition to the variables defined in table 1,

$$\boldsymbol{P}_f = p_f\boldsymbol{I} + \rho_f\boldsymbol{R}_f \qquad \boldsymbol{R}_f = 2k_f\left(\frac{1}{3}\boldsymbol{I} + \boldsymbol{b}\right) \qquad \varepsilon_{PT} = C_f k_f^{3/2}/d_p$$

$$S_E = \max(S_a, 0)\left(\frac{1}{2}u_f^2 + k_f\right) + \min(S_a, 0)E_p$$

$$D_E = K\left[\boldsymbol{u}_p\cdot\boldsymbol{u}_{pf} + 3a\Theta_p - 2(1-a)k_f\right] \qquad D_{PT} = K\left[u_{fp}^2 + 3a\Theta_p - 2(1-a)k_f\right]$$

$$\Theta_f = (\gamma_f - 1)\left(E_f - \frac{1}{2}u_f^2 - k_f\right) \qquad a = \frac{1 + Z\alpha_a}{1 + Z(\alpha_f\alpha_p b + \alpha_a)} \qquad Z = \rho_f/\rho_p$$

TABLE 2. Compressible two-fluid model for particles in a fluid modelled as a stiffened gas with a transport equation for pseudo-turbulent kinetic energy (PTKE) k_f. The pseudo-turbulence tensor $\boldsymbol{R}_f$ arises due to the finite-size of the particles and $\boldsymbol{b}$ is the PTKE anisotropy tensor (Tenneti *et al.* 2011). The model for a is based on the asymptotic behaviours for $\rho_f = 0$ and $\rho_p = 0$. The parameter b fixes the ratio $3\Theta_p/2k_f$ when $\rho_p = 0$, and direct-numerical simulation data (Tavanashad *et al.* 2019) suggest that $b = 0.365$. The constant C_f is order one and fixes the magnitude of k_f in spatially homogeneous flow (Shallcross *et al.* 2020). An alternative is to use a transport equation for ε_{PT} to account for the integral length scale of PTKE in lieu of d_p.

Hereinafter, we define the variable c_m such that $\alpha_a = c_m\alpha_f\alpha_p$, which is a convenient form to enforce the upper limit on α_a.

Although its definition is not required to analyse the hyperbolicity, the added-mass exchange rate will be approximated by a linear relaxation model:

$$S_a = \frac{\rho_f\alpha_f\alpha_p}{\tau_a}(c_m^\star - c_m) \tag{2.5}$$

with time scale

$$\tau_a = \frac{4d_p^2\alpha_f^\star}{3\nu_f C_D Re_p \alpha_f}. \tag{2.6}$$

Physically, τ_a is the time scale characterizing the expansion/contraction/formation of particle wakes. For example, when a particle moves from a region with large α_p to one with small α_p (i.e. to larger spacing between particles), c_m will be smaller than $c_m^\star$. Thus, the wake will grow by entraining fluid with velocity $\boldsymbol{u}_f$ and kinetic energy $\frac{1}{2}u_f^2 + k_f$. The time scale in (2.6) is meant to estimate this rate of growth and can be further refined using data from particle-resolved direct-numerical simulations (PRDNS) (see, e.g., Moore & Balachandar 2019) .

2.3. *Added-mass function*

In principle, by formulating a physically accurate function for $c_m^\star$, the two-fluid model will be able to account correctly for unsteady effects. For example, $c_m^\star$ might depend on Ac (Odar & Hamilton 1964), making the added mass of the particle larger when the particle acceleration is high. In this work, we are primary interested in the effect of added mass on the hyperbolicity of the two-fluid model. In this context, source terms that do not depend on space or time derivatives (such as S_a) have no influence on the eigenvalues of the flux matrix. Nonetheless, the added-mass function $c_m^\star(x)$ must have the properties $0 \leqslant \alpha_p c_m^\star \leqslant 1$ and $c_m^\star(0) = C_m$ where C_m is the added-mass constant, which is equal to $1/2$ for a spherical particle when $\alpha_p = 0$ (Zuber 1964). In addition, one might require $c_m^\star(1) = 1$ to force all of the fluid phase to be treated as added mass when its volume fraction approaches zero, but this is not required for hyperbolicity.

Theoretical expressions for the dependence of added mass on the particle volume fraction can be found in Sangani *et al.* (1991); however, these expressions are valid for $\alpha_p < 0.5$. From the hyperbolicity analysis in §3, we find that $0.085 < c_m^\star < 1/\alpha_p$, which corresponds physically to $0 < \alpha_f^\star < \alpha_f$. These observations suggest the use of the expression proposed by Zuber (1964) (written to account for the difference between $\boldsymbol{u}_f$ and $\boldsymbol{v}_f$) of the form

$$c_m^\star = \frac{1}{2}\min\left(1 + 2\alpha_p, 2\right). \tag{2.7}$$

Sangani *et al.* (1991) showed that this form is suitable for most applications (e.g. bubble and spherical particles with no-slip and free-slip boundaries); hence, it will be the default expression in the proposed two-fluid model. Nonetheless, as done in Moore & Balachandar (2019) for the velocity wakes around Lagrangian particles, PRDNS could be used to improve this model to account for the particle Reynolds number and volume fraction dependencies.

Another possible expression (which allows for direct computation of $\alpha_p^\star$ versus α_p) is the linear form

$$c_m^\star = C_m + (1 - C_m)x \tag{2.8}$$

with $x = \alpha_p$ or $x = \alpha_p^\star$, and $0 \leqslant C_m \leqslant 2$. Based on their experimental results, Odar & Hamilton (1964) found that C_m depends on the acceleration number as

$$C_m = 1 - \frac{1}{2}e^{-\beta Ac} \tag{2.9}$$

where $\beta \approx 3$ and the acceleration number is defined by $Ac = 4/(3C_D)$. Thus, for very slow acceleration, $C_m = 1/2$, whereas for rapid acceleration $C_m = 1$. However, more recent theoretical works (e.g., Auton *et al.* 1988; Sangani *et al.* 1991; Mei & Adrian 1992) suggest that the decomposition of the virtual-mass and history forces used by

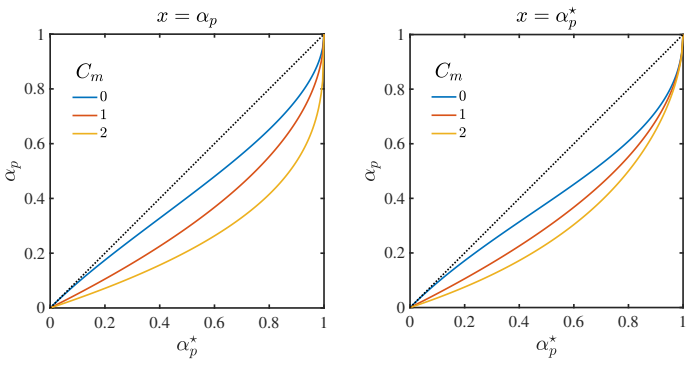

FIGURE 2. Steady-state relation between α_p and $\alpha_p^\star$ for the added-mass function $c_m^\star = C_m + (1 - C_m)x$ with three values of C_m. Left: $x = \alpha_p$. Right: $x = \alpha_p^\star$. The diagonal line corresponds to $c_m^\star = 0$. For the function in (2.7), the dependence will be the same as $C_m = 1$ for $1/2 < \alpha_p$. Note that the curve for $C_m = 1$ is the same for both choices of x.

Odar & Hamilton (1964) is not reliable, and that $C_m = 1/2$ independent of Ac. In any case, using (2.8) and given that $\alpha_p^\star = \alpha_p + c_m\alpha_p(1-\alpha_p)$, at steady state where $c_m = c_m^\star$ with $x = \alpha_p$, the value of α_p is the root in the interval [0 1] of a cubic polynomial for $0 \leqslant C_m \leqslant 2$:

$$(1 - C_m)\alpha_p^3 + (2C_m - 1)\alpha_p^2 - (C_m + 1)\alpha_p + \alpha_p^\star = 0. \tag{2.10}$$

For $C_m = 1$, the desired root is $\alpha_f^2 = \alpha_f^\star$ (which also holds for (2.7) when $\alpha_f < 1/2$). For other values of C_m, the root can be found numerically as illustrated in figure 2.

As previously noted, the choice of $c_m^\star$ has no effect on the hyperbolicity of the two-fluid model. Notwithstanding this fact, for actual applications, it will be important to choose a functional form that accurately matches the dependence of the added mass on α_p, etc., derived from PRDNS, experiments, and theory.

2.4. *Particle-phase pressure tensor*

In fluid–particle flows, the particles have uncorrelated motion due to fluid-mediated interactions and direct collisions (Lhuillier *et al.* 2013). In recent PRDNS studies of bubbly flow (du Cluzeau *et al.* 2019, 2020), these fluctuations are referred to as the dispersed-phase Reynolds stresses, but it is important to note that they are present in purely laminar flows (Biesheuvel & van Wijngaarden 1984). Indeed, in kinetic theory the magnitude of the dispersed-phase Reynolds stresses is proportional to the granular temperature Θ_p. In du Cluzeau *et al.* (2020), it is found that these terms (referred to as $\boldsymbol{M}^{extra}$ and $\boldsymbol{M}^{LD}$) make a significant contribution to the dispersed-phase momentum balance. As described by these authors, in two-fluid models the corresponding flux terms in the dispersed-phase momentum balance are usually separated into 'dispersion' forces (proportional to $\partial_{\mathbf{x}}\alpha_p$) and a 'drag' force contributions. However, from the standpoint of examining the hyperbolicity of the two-fluid model, it is simplest to treat them as part of the momentum flux as done in this work.

Considering the effective repulsive force exerted between particles in random motion, Batchelor (1988) proposed a (one-dimensional) particle-phase stress model written in terms of the hydrodynamic diffusivity D and the bulk mobility B of the form (written

in our notation)

$$\partial_x p_p = \partial_x \alpha_p \rho_p \Theta_p - \frac{\rho_p D}{m_p B} \partial_x \alpha_f \tag{2.11}$$

where m_p is the particle mass. He then used physical reasoning to argue that

$$\frac{\rho_p D}{m_p B} \propto \rho_f u_{fp}^2. \tag{2.12}$$

Considering that Batchelor's model was developed for a 1-D flow with an incompressible fluid phase, it is not unreasonable to treat his dispersion term as part of the particle pressure as done in our compressible two-fluid model. From the kinetic-theory derivation (Fox 2019), a dispersion term is also found in $\boldsymbol{F}_{pf}$, but written in terms of $\partial_{\mathbf{x}} \rho_f$ and not $\partial_{\mathbf{x}} \alpha_f$. Thus, this dispersion term would be zero for an incompressible fluid phase. Mathematically, the dispersion term in (2.11) would appear with the opposite sign in the fluid momentum balance (i.e., it would be an interphase force), and the mixture momentum balance would only contain p_p.

Syamlal (2011) derived a 'buoyant-force' term that extends the fluid pressure in the Archimedes force to include a relative-velocity contribution of the form $\rho_f \alpha_f \boldsymbol{u}_{fp} \otimes \boldsymbol{u}_{fp}$. Neglecting the particle pressure and considering an incompressible fluid, he demonstrates that the two-fluid model for mass and momentum with this additional force is hyperbolic. Comparing his model to the one in table 1 (and ignoring added mass), we observe that the term in the fluid-phase momentum flux involving $\boldsymbol{R}$ (which is exact from kinetic theory (Fox 2019)) is not present, and the particle-phase pressure tensor term $\partial_{\mathbf{x}} \cdot (\alpha_a \boldsymbol{P}_{fp}^a)$ is replaced by the buoyant-force term $\alpha_p \partial_{\mathbf{x}} \cdot (\rho_f \alpha_f \boldsymbol{u}_{fp} \otimes \boldsymbol{u}_{fp})$. In §3.2, we find that the $\boldsymbol{R}$ contribution to the fluid-phase momentum flux is not required for hyperbolicity (and, for constant ρ_f, can be combined with the fluid pressure as done in §5.2). Thus, by rewriting the buoyant-force term in the form

$$\alpha_p \partial_{\mathbf{x}} \cdot (\rho_f \alpha_f \boldsymbol{u}_{fp} \otimes \boldsymbol{u}_{fp}) = \partial_{\mathbf{x}} \cdot (\rho_f \alpha_f \alpha_p \boldsymbol{u}_{fp} \otimes \boldsymbol{u}_{fp}) - \rho_f \alpha_f (\boldsymbol{u}_{fp} \otimes \boldsymbol{u}_{fp}) \cdot \partial_{\mathbf{x}} \alpha_p, \tag{2.13}$$

it can be interpreted as a combination of a fluid-mediated particle-phase pressure tensor and a dispersion force, albeit with a negative coefficient. As we show in §3, the fluid-mediated particle-phase pressure is essential for ensuring a hyperbolic system.

Zhang *et al.* (2006) and Zhang (2020) derived a two-fluid formulation from a general kinetic theory accounting for long-range particle–particle interactions. A particle–fluid–particle (PFP) force of the form $\partial_{\mathbf{x}} \cdot (\alpha_p \boldsymbol{\Sigma}_{pfp})$, where $\boldsymbol{\Sigma}_{pfp}$ is the PFP stress, appears in their formulation. For uniform potential flow with constant ρ_f, Zhang (2020) finds that

$$\alpha_p \boldsymbol{\Sigma}_{pfp} = \rho_f [C_1(\alpha_p) u_{fp}^2 \boldsymbol{I} + C_2(\alpha_p) \boldsymbol{u}_{fp} \otimes \boldsymbol{u}_{fp}] \tag{2.14}$$

where C_1 and C_2 are coefficients that can be determined numerically. Unlike in (2.13), no dispersion term arises in addition to the PFP force, nor is $\boldsymbol{\Sigma}_{pfp}$ related to the Archimedes force. Nevertheless, the stress tensor in (2.13) is a special case of (2.14) and, hence, it is reasonable to expect that the PFP force would affect favourably the hyperbolicity of the system (which depends on the trace of $\boldsymbol{\Sigma}_{pfp} \propto \rho_f u_{fp}^2$).

In kinetic theory, the dispersed-phase Reynolds stresses and fluid-mediated interactions contribute to the particle-phase pressure tensor. Thus, from a physical-modelling standpoint, an important component in the two-fluid model is the closure for this term:

$$\boldsymbol{P}_p = p_p \boldsymbol{I} + \alpha_a \boldsymbol{P}_{fp}^a \tag{2.15}$$

where $p_p = \alpha_p p_p^k + \alpha_a p_f^a$ with $p_p^k = \rho_p \Theta_p \left(1 + 4\alpha_p^\star g_0\right)$, $p_f^a = \rho_f \Theta_p \left(1 + 4\alpha_p^\star g_0\right)$ and

$$\boldsymbol{P}_{fp}^a = \rho_f \frac{2}{3\gamma_p} \left(\frac{1}{2} u_{fp}^2 \boldsymbol{I} + \boldsymbol{u}_{fp} \otimes \boldsymbol{u}_{fp} \right) \left(1 + 4\alpha_p^\star g_0\right), \tag{2.16}$$

which is a particular form of (2.14). This model for $\boldsymbol{P}_p$ combines the kinetic-theory dependence on Θ_p due to uncorrelated velocity fluctuations and direct collisions when $\rho_f \ll \rho_p$ (i.e. p_p) with a component to describe the fluid-mediated interactions between particles *that are taken to be proportional to the added mass*. In other words, even when the granular temperature is null, in order to have a globally hyperbolic system we assume that a particle pressure exists due to interactions between the particles via the fluid phase (see van Wijngaarden 1976; Batchelor 1988; Zhang *et al.* 2006; Zhang 2020, for detailed discussions).

In (2.16), the contribution $1 + 4\alpha_p^\star g_0$ with $1 \leqslant g_0$ accounts for the excluded volume occupied by the particles. Other formulations of (2.16) are possible and will perhaps be required to capture the correct physics (e.g., when $\rho_f \approx \rho_p$ or for deformable particles such as bubbles). For example, one might consider replacing $\alpha_p^\star g_0$ with $\alpha_p g_0$, or changing altogether the definition of g_0. However, as shown in §3, such changes will not affect the hyperbolicity of the compressible two-fluid model as long as γ_p is not so large as to make $\boldsymbol{P}_{fp}^a$ negligible. Furthermore, in §3 we find that with $\alpha_p = 0$, the system is hyperbolic even when $c_m = 0$ (i.e., $\alpha_a = 0$ in (2.15)). Thus, it is possible for $\boldsymbol{P}_{fp}^a$ in (2.16) to depend linearly on $\alpha_p^\star$ (so that the fluid-mediated pressure depends on α_p^2) without changing the hyperbolicity of the system. An example of this behaviour is presented in appendix B where it is shown that for an incompressible fluid the two-fluid model with $trace(\alpha_a \boldsymbol{P}_{fp}^a) \propto (\alpha_p^\star)^2 u_{fp}^2$ is globally hyperbolic.

The tensorial form of the fluid-mediated particle pressure in (2.16), and its appearance with the opposite sign in the fluid-phase momentum balance, is motivated as follows. In the kinetic-theory derivation of Fox (2019), it was shown that the mixture pressure tensor has the form $\boldsymbol{P}_{mix} = \boldsymbol{P}_1 + \boldsymbol{P}_2 + c_{12}\boldsymbol{P}_{BE}$ regardless of the size ratio between the hard spheres. The Boltzmann–Enskog contribution $\boldsymbol{P}_{BE}$ leads to the term involving $\boldsymbol{R}$ in the fluid-phase momentum balance when added mass is neglected ($\alpha_a = 0$). Biesheuvel & van Wijngaarden (1984) derive a contribution to the mixture stress and liquid-phase Reynolds stresses with the same tensorial form as $\boldsymbol{R}$ based on potential flow around spherical bubbles, but neglecting particle–particle interactions. Thus, with added mass, we assume that the mixture pressure tensor remains unchanged, and share the contribution $\alpha_a \boldsymbol{P}_{fp}^a$ between the two phases. This is consistent with the kinetic-theory derivation where the particle pressures in each phase depend on the particle size ratio, while the mixture pressure does not (Fox 2019). Finally, note that the contribution $\partial_{\mathbf{x}} \cdot (\alpha_a \boldsymbol{P}_{fp}^a)$ arises from the kinetic-theory derivation as a modification to the pressure tensors, while in the compressible two-fluid model it can be interpreted as a fluid-mediated exchange force. Finally, the parameter γ_p in (2.16) is equal to 5/3 for hard-sphere in an ideal gas, but in general it can be used as a parameter to set the magnitude of the fluid-mediated particle pressure (i.e. $tr(\boldsymbol{P}_{fp}^a) \propto 5/(3\gamma_p)$). On the other hand, the tensorial form of $\boldsymbol{P}_{fp}^a$ must be kept consistent with that of $\boldsymbol{R}$ as both arise due from the same term in the kinetic-theory derivation (Fox 2019). As seen from (2.14), up to the scalar coefficients that can depend on α_p, this tensorial form is the only one that can be formed from $\boldsymbol{u}_{fp}$ (Zhang 2020).

In summary, the particle-pressure tensor in (2.15) combines two limiting behaviours for the material-density ratio and it is a key modelling component for ensuring hyperbolicity when $\rho_p \ll \rho_f$. This is consistent with Batchelor (1988) where it is also shown to have a strong effect on the linear stability of a uniform suspension. It is also consistent with the

kinetic-theory derivation of Zhang *et al.* (2006); Zhang (2020) who demonstrate that an inter-species stress arises due to particle–fluid–particle interactions, which do not depend on Θ_p. Nonetheless, future research should be devoted to refining the model for $\alpha_a \boldsymbol{P}^a_{fp}$ in (2.16) to account for the α_p and Re_p dependencies observed in PRDNS.

2.5. *Limiting cases*

Having previously investigated the case with $\rho_f \ll \rho_p$ (Fox 2019), in the remainder of this work we are particularly interested in the limiting cases with $\rho_p = 0$ (i.e., the particles have zero mass) so that $\rho_e \alpha_p^\star = \rho_f \alpha_a$. However, we will also analyse the hyperbolicity of the complete model for selected values of the material density ratio Z. As is well known, the drag and body forces appearing on the right-hand sides of the model equations do not affect the eigenvalues of the two-fluid model. Hence, in §3 we will ignore them and consider only the terms involving temporal and spatial gradients.

3. Hyperbolicity of 1-D two-fluid model

In order to determine whether the full 3-D model in table 2 is hyperbolic, it suffices to consider a system with one spatial direction (see, e.g., Lhuillier *et al.* 2013; Ndjinga 2007; Kumbaro & Ndjinga 2011). This approach will be followed here, starting with the 1-D model without source terms that do not involve temporal or spatial derivatives.

3.1. *1-D compressible two-fluid model*

The 1-D model without the source terms is given in table 3, written in terms of eight independent variables:

$$\mathbf{X} := (X_1, X_2, X_3, X_4, X_5, X_6, X_7, X_8)^t = (\alpha_p, \rho_e \alpha_p^\star / \rho_p, Z\alpha_f^\star, u_p, u_f, E_p, E_f, k_f)^t. \quad (3.1)$$

We define Z such that $\rho_f = Z\rho_p$. As ρ_p is constant, it can be factored out of the model if desired. The conserved variables (X_1, X_2, X_3) are related to $(\alpha_p, Z, \alpha_f^\star)$ by

$$\alpha_p = X_1, \quad Z = \frac{X_3 + X_2 - X_1}{\alpha_f}, \quad \alpha_f^\star = \frac{X_3}{Z}, \quad (3.2)$$

and all other variables appearing in the momentum and energy balances can be found from these variables. In addition to the model in table 3, we will also analysis the simplified model given in table 4, which neglects the Boltzmann–Enskog fluxes (i.e., $\boldsymbol{R}$ and $\boldsymbol{r}$ in the fluid phase) and forces (i.e., $\boldsymbol{F}_{fp}$ and D_{fp}) that are specific to hard-sphere mixtures (Fox 2019).

Formally, the 1-D models can be rewritten as

$$\mathbf{A}(\mathbf{X})\partial_t \mathbf{X} + \mathbf{B}(\mathbf{X})\partial_x \mathbf{X} = \mathbf{0} \quad (3.3)$$

where the coefficient matrices $\mathbf{A}$ and $\mathbf{B} := \mathbf{B}^* + \mathbf{B}_0$ yield the flux matrix $\boldsymbol{F} := \mathbf{A}^{-1}\mathbf{B}$. Here, $\mathbf{B}_0$ is the contribution due to the pressure and buoyancy terms, and $\mathbf{A}$ and $\mathbf{B}^*$ are from the convection terms. Written in terms of the components of $\mathbf{X}$, the latter are

$$\mathbf{A} := \begin{bmatrix} 1 & 0 & 0 & 0 & 0 & 0 & 0 & 0 \\ 0 & 1 & 0 & 0 & 0 & 0 & 0 & 0 \\ 0 & 0 & 1 & 0 & 0 & 0 & 0 & 0 \\ 0 & 0 & 0 & X_2 & 0 & 0 & 0 & 0 \\ 0 & 0 & 0 & 0 & X_3 & 0 & 0 & 0 \\ 0 & 0 & 0 & 0 & 0 & X_2 & 0 & 0 \\ 0 & 0 & 0 & 0 & 0 & 0 & X_3 & 0 \\ 0 & 0 & 0 & 0 & 0 & 0 & 0 & 1 \end{bmatrix} \quad (3.4)$$

$$\partial_t X_1 + \partial_x(X_1 X_4) = 0$$
$$\partial_t X_2 + \partial_x(X_2 X_4) = 0$$
$$\partial_t X_3 + \partial_x(X_3 X_5) = 0$$
$$X_2(\partial_t + X_4\partial_x)X_4 + \partial_x(p_p + \alpha_a P^a_{fp}) + \alpha^\star_p \partial_x P_f + F_{pf} = 0$$
$$X_3(\partial_t + X_5\partial_x)X_5 + \partial_x(\alpha^\star_p Z R - \alpha_a P^a_{fp}) + \alpha^\star_f \partial_x P_f - F_{pf} = 0$$
$$X_2(\partial_t + X_4\partial_x)X_6 + \partial_x(p_p X_4) + X_4\partial_x(\alpha_a P^a_{fp}) + X_4\alpha^\star_p\partial_x P_f + D_{pf} = 0$$
$$X_3(\partial_t + X_5\partial_x)X_7 + \partial_x(\alpha^\star_f P_f X_5 + \alpha^\star_p Z R X_4 + r) - X_4\partial_x(\alpha_a P^a_{fp}) + P_f\partial_x(\alpha^\star_p X_4) - D_{pf} = 0$$
$$(\partial_t + X_5\partial_x)X_8 + 2X_8\partial_x X_5 = 0$$

where

$$\alpha_p = X_1 \quad Z = \frac{X_2 + X_3 - X_1}{\alpha_f} \quad \alpha^\star_f = \frac{X_3}{Z} \quad \alpha_f = 1 - \alpha_p \quad \alpha^\star_p = 1 - \alpha^\star_f \quad \alpha_a = \alpha^\star_p - \alpha_p$$

$$R = \Theta_p + \frac{1}{\gamma_p}(X_4 - X_5)^2 \qquad p_f = Z\Theta_f - \gamma_f(\gamma_f - 1)Z_0 p^\star_o \frac{\alpha_f}{\alpha^\star_f} \qquad p_p = (\alpha_p + Z\alpha_a)\Theta_p(1 + 4\alpha^\star_p g_0)$$

$$P_f = p_f + 2ZX_8 \qquad P^a_{fp} = \frac{Z}{\gamma_p}(X_4 - X_5)^2(1 + 4\alpha^\star_p g_0) \qquad r = 2Z\alpha^\star_p\Theta_p(X_4 - X_5)$$

$$F_{pf} = \alpha^\star_p R\partial_x Z + (\gamma_p - 1)\alpha^\star_p Z(X_5 - X_4)\partial_x X_5 \qquad D_{pf} = X_4 F_{pf} + 2\alpha^\star_p\Theta_p[(X_4 - X_5)\partial_x Z - Z\partial_x X_5]$$

$$\Theta_f = (\gamma_f - 1)\left(X_7 - \frac{1}{2}X_5^2 - X_8\right) \qquad \Theta_p = (\gamma_p - 1)\left(X_6 - \frac{1}{2}X_4^2\right) \qquad g_0 = \frac{1 + \alpha_f}{2\alpha_f^3}$$

TABLE 3. One-dimensional compressible two-fluid model with the densities, pressures, fluxes and forces normalized by ρ_p. The reference pressure $p^\star_o$ is constant and has the same units as Θ_f, and the Z_0 is the reference density ratio.

and

$$\mathbf{B}^* := \begin{bmatrix} X_4 & 0 & 0 & X_1 & 0 & 0 & 0 & 0 \\ 0 & X_4 & 0 & X_2 & 0 & 0 & 0 & 0 \\ 0 & 0 & X_5 & 0 & X_3 & 0 & 0 & 0 \\ 0 & 0 & 0 & X_2X_4 & 0 & 0 & 0 & 0 \\ 0 & 0 & 0 & 0 & X_3X_5 & 0 & 0 & 0 \\ 0 & 0 & 0 & 0 & 0 & X_2X_4 & 0 & 0 \\ 0 & 0 & 0 & 0 & 0 & 0 & X_3X_5 & 0 \\ 0 & 0 & 0 & 0 & 2X_8 & 0 & 0 & X_5 \end{bmatrix}. \tag{3.5}$$

The components of $\mathbf{B}_0$ are more complex due to the non-linearities, but can easily be computed using symbolic software, as can the flux matrix and its characteristic polynomial. Due to the non-linearities of the additional fluxes and forces in the full versus the simplified model, the latter can be analysed analytically in greater detail. Nonetheless, it is always possible to compute the eigenvalues numerically in order to check the predictions of the analysis.

The eight eigenvalues of $\boldsymbol{F}$ can be written $u_f + u_0\lambda_k$ with $k \in \{1, \ldots, 8\}$, where for fixed values of $\overline{p^o_f} = \frac{Z_0 p^\star_o}{u_0^2} = \frac{p^o_f}{\rho_p u_0^2}$, γ_f and γ_p, each λ_k, called here a normalized eigenvalue, depends on five dimensionless parameters:

$$\alpha_p, \quad c_m, \quad Ma_s = \frac{u_p}{u_0}, \quad \Theta_r = \frac{\Theta_p}{u_0^2} \quad K_r = \frac{k_f}{u_0^2}, \tag{3.6}$$

$$\partial_t X_1 + \partial_x(X_1 X_4) = 0$$
$$\partial_t X_2 + \partial_x(X_2 X_4) = 0$$
$$\partial_t X_3 + \partial_x(X_3 X_5) = 0$$
$$X_2(\partial_t + X_4\partial_x)X_4 + \partial_x(p_p + \alpha_a P^a_{fp}) + \alpha^\star_p \partial_x P_f = 0$$
$$X_3(\partial_t + X_5\partial_x)X_5 - \partial_x(\alpha_a P^a_{fp}) + \alpha^\star_f \partial_x P_f = 0$$
$$X_2(\partial_t + X_4\partial_x)X_6 + \partial_x(p_p X_4) + X_4\partial_x(\alpha_a P^a_{fp}) + X_4\alpha^\star_p\partial_x P_f = 0$$
$$X_3(\partial_t + X_5\partial_x)X_7 + \partial_x(\alpha^\star_f P_f X_5) - X_4\partial_x(\alpha_a P^a_{fp}) + P_f\partial_x(\alpha^\star_p X_4) = 0$$
$$(\partial_t + X_5\partial_x)X_8 + 2X_8\partial_x X_5 = 0$$

where

$$\alpha_p = X_1 \qquad Z = \frac{X_2 + X_3 - X_1}{\alpha_f} \qquad \alpha^\star_f = \frac{X_3}{Z}$$

$$\alpha_f = 1 - \alpha_p \qquad \alpha^\star_p = 1 - \alpha^\star_f \qquad \alpha_a = \alpha^\star_p - \alpha_p \qquad P^a_{fp} = \frac{Z}{\gamma_p}(X_4 - X_5)^2(1 + 4\alpha^\star_p g_0)$$

$$P_f = p_f + 2ZX_8 \qquad p_f = Z\Theta_f - \gamma_f(\gamma_f - 1)Z_0 p^\star_o \frac{\alpha_f}{\alpha^\star_f} \qquad p_p = (\alpha_p + Z\alpha_a)\Theta_p(1 + 4\alpha^\star_p g_0)$$

$$\Theta_f = (\gamma_f - 1)\left(X_7 - \frac{1}{2}X_5^2 - X_8\right) \qquad \Theta_p = (\gamma_p - 1)\left(X_6 - \frac{1}{2}X_4^2\right) \qquad g_0 = \frac{1 + \alpha_f}{2\alpha^3_f}$$

TABLE 4. Simplified version of 1-D compressible two-fluid model from table 3. This model is hyperbolic when the fluid-phase eigenvalues are sufficiently separated from those for the particle phase. When this is not the case, the kinetic-theory terms in the full model may be needed to achieve hyperbolicity.

where $\Theta_f = u_0^2 + \Theta_0$ and Θ_0 is defined by $p_f = 0$ from the stiffened-gas model. The parameter Θ_0 depends on Z. The λ_k are the roots of $P(X) = Q(u_0 X)/u_0^8$, where Q is the characteristic polynomial of $\boldsymbol{F} - u_f \boldsymbol{I}$. In general, in order for the eigenvalues to be real, p_f must be positive. The characteristic velocity u_0 should not be confused with the speed of sound in the stiffened-gas model, which scales like $c_f = (\gamma_f p^o_f)^{1/2}$ and is orders of magnitude larger than u_0. For the model in table 3, there are two normalized eigenvalues that can be computed analytically, namely, 0 and Ma_s. For the model in table 4, there is an additional normalized eigenvalue at Ma_s. In general, the remaining normalized eigenvalues in both models depend on the five parameters in (3.6).

For $\alpha_p = 0$, the normalized eigenvalues (which are the same for both models) can be computed analytically:

$$0, \quad \pm\sqrt{\gamma_f + \gamma_f(\gamma_f - 1)\frac{\overline{p^o_f}}{Z} + 6K_r}, \quad Ma_s,$$
$$\frac{1 + (1 + 1/\gamma_p)c_m Z}{1 + c_m Z} Ma_s \pm \sqrt{\frac{(1 + (1 + 1/\gamma_p^2)c_m Z)c_m Z}{(1 + c_m Z)^2} Ma_s^2 + \gamma_p \Theta_r} \quad (3.7)$$

and are always real valued, including when $c_m = 0$. Here, the two 'fluid-phase' eigenvalues that depend on $\overline{p^o_f}$ are always real and distinct. Note that when $\Theta_r = 0$ the 'particle-phase' eigenvalues scale with Ma_s, but always remain real-valued. When $Ma_s = 0$, these eigenvalues depend on Θ_r like an ideal gas ($\gamma_p = 5/3$). In the following, we investigate the behaviour of the eigenvalues for a stiffened gas ($\gamma_f = 29/4$) with fixed values of Z,

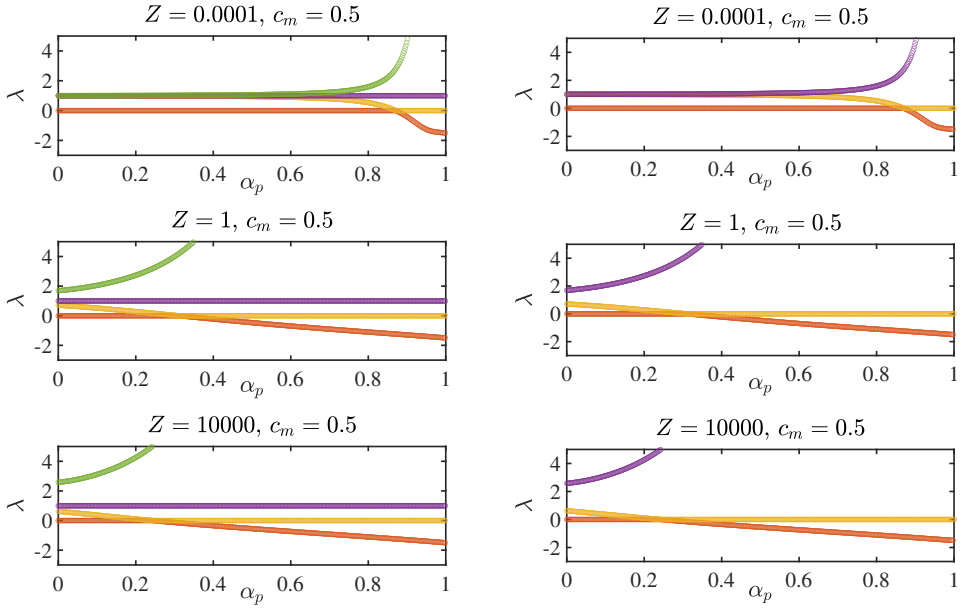

FIGURE 3. Normalized eigenvalues dependent on α_p for the full (left) and simplified (right) 1-D models. The two eigenvalues dependant on $p_o^\star = 10^8$, and the eigenvalue at Ma_s for the simplified model, are not shown. All eigenvalues are real valued with these parameters as shown in §3.2.

namely, $+\infty$, 1, and 0; which correspond, respectively, to bubbly, neutrally buoyant and granular flow. The behaviour of the eigenvalues for other values of Z can be inferred from these limiting cases. For the model in table 3, there will be six eigenvalues that vary with α_p, as opposed to five for the model in table 4. From the examples in figure 3, it can be observed that the differences between the full and simplified model are small. The magnitudes of the two 'particle-phase' eigenvalues increase with α_p mainly due to g_0, while their values at $\alpha_p = 0$ depend on c_m as shown in (3.7).

3.2. *Hyperbolicity analysis of simplified model*

For the simplified model in table 4, a theoretical study of the hyperbolicity can be carried out analytically. As done in Chalons *et al.* (2017), Sturm's theorem (Sturm 1829) can be used, which determines the number of distinct real roots in a given interval. For that, let us consider the polynomial $P_0 = P/(X(X - Ma_s)^2)$, where P is the polynomial defined above. The Sturm sequence of polynomials is defined by P_0, $P_1 = P_0'$ and, for any $n \in \{0, 1, 2, 3\}$, $-P_{n+2}$ is the remainder of the Euclidean division of P_{n+1} by P_n. With the use of symbolic software, one can compute this sequence. If the coefficient S_n of the highest-order term of each P_n, called hereinafter a Sturm's coefficient, is positive for $n \in \{0, 1, \ldots, 5\}$, then Q has five real roots, meaning that all eigenvalues of the system are real.

In the general case, it is hard to prove that all the Sturm's coefficients S_n are positive. However, since c_f is large compared to u_0, the limit when c_f tends to infinity can be studied, i.e., for a very large value of $\overline{p_f^o}$. Thus, a Taylor expansion of the S_n can be done when $\epsilon = 1/\overline{p_f^o}$ tends to zero, for $\gamma_f = 29/4$ and $\gamma_p = 5/3$. Then, $S_0 = 1$, $S_1 = 6$ and the

limit of ϵS_n when ϵ tends to zero is studied:

$$\epsilon S_2 \to \frac{145}{8}\frac{\alpha_f(1+c_mZ)+\alpha_pZ}{\alpha_fZ(\alpha_fc_mZ+1)(1-c_m\alpha_p)}$$

$$\epsilon S_3 \to \frac{2175}{16}\frac{\alpha_f+Z\alpha_p+\alpha_fc_mZ}{\alpha_fZ(\alpha_fc_mZ+1)(1-c_m\alpha_p)}$$

$$\epsilon S_4 \to \Theta_r\frac{p_2(\alpha_f,c_m,Z)}{1-c_m\alpha_p}+Ma_s^2\frac{p_1(\alpha_f,c_m,Z)}{(1-c_m\alpha_p)^3}\left\{5\alpha_f^8(1-c_m\alpha_p)^2+c_mZ^2q_1(\alpha_f,c_m)\right.$$
$$\left.+Z(1-c_m\alpha_p)[18\alpha_f^5\alpha_pc_m^2(1+\alpha_f)(1-c_m\alpha_p)+q_2(\alpha_f,c_m)]\right\}$$

$$\epsilon S_5 \to \frac{\mu(\alpha_p,c_m,Z,Ma_s,\Theta_r)^2}{(1-c_m\alpha_p)}\left\{\Theta_rp_3(\alpha_f,c_m,Z)+Ma_s^2\left[c_mZ^2q_4(\alpha_f,c_m)\right.\right.$$
$$\left.\left.+5(1+\alpha_fc_mZ)[q_3(\alpha_f,c_m)+6c_m^2\alpha_f^5\alpha_p(1-\alpha_f)(1-c_m\alpha_p)]\right]\right\}$$

where each $p_k(\alpha_f,c_m,Z)$ is a polynomial function of α_f, c_m and Z that is positive for $\alpha_f \in [0,1]$, $c_m \geqslant 0$ and $Z \geqslant 0$, each $q_k(\alpha_f,c_m)$ is a polynomial function of α_f and c_m that is positive for $\alpha_f \in [0,1]$ if c_m is large enough, a sufficient condition being $c_m > 0.085$. Moreover, μ is a function of the parameters $(\alpha_p,c_m,Z,Ma_s,\Theta_r)$. Then the limits of the ϵS_k are positive as long as $1-c_m\alpha_p > 0$, and if neither c_m nor Θ_r are too small, $c_m > 0.085$ being a sufficient condition. The simplified model is then hyperbolic in those cases in the limit of infinite $\overline{p_f^o}$.

3.3. *Eigenvalues for specific cases*

We are specifically interested to know whether the 1-D models are hyperbolic for all physically relevant values of $0 \leqslant \alpha_p \leqslant 1$ and $0 \leqslant c_m \leqslant 1/\alpha_p$. As can be seen in (3.7), K_r mainly affects the 'fluid-phase' eigenvalues, so it suffices to show hyperbolicity for $K_r = 0$. Similarly, Θ_r mainly affects the 'particle-phase' eigenvalues and $\Theta_r = 0$ is known to yield complex eigenvalues when added mass is neglected (Fox 2019); hence, the analysis of this limiting case is of particular interest. As done in Fox (2019), we will make use of stability plots found from the Sturm coefficients to check for complex eigenvalues in α_p–c_m parameter space.

3.3.1. *Granular flow with $\rho_f = 0$*

The limit $Z = 0$ corresponds to a granular flow with $\rho_f = 0$. For this case, the 1-D model is globally hyperbolic. Nonetheless, the hyperbolicity plot in figure 4 requires a Ma_s-dependent minimum value for Θ_r due to round-off errors in evaluating the Sturm coefficients. As can be seen in figure 3 and from (3.7), the particle phase has multiple eigenvalues at Ma_s when $Z = 0$ and $\Theta_r = 0$.

3.3.2. *Neutrally buoyant flow with $\rho_p = \rho_f$*

The limit $Z = 1$ corresponds to a neutrally buoyant flow with $\rho_p = \rho_f$. From the hyperbolicity plot in figure 5, we can observe that the models are hyperbolic except for a small region near $c_m = 0$. In other words, there is a minimum value of c_m above which the models are globally hyperbolic. Note that this value is significantly smaller than the standard added-mass constant $c_m = 1/2$. In figure 6, examples with complex eigenvalues corresponding to small c_m are shown. It can be observed that with $Z = 1$ the eigenvalues for the two models are quite similar unless c_m is very small. It is noteworthy that when c_m is small enough, the 'disturbance' eigenvalue that begins above unity at $\alpha_p = 0$ can be less that unity for values of α_p near 0.15. In other words, particle-phase disturbances propagate more slowly than the mean slip velocity if the added mass is relatively small.

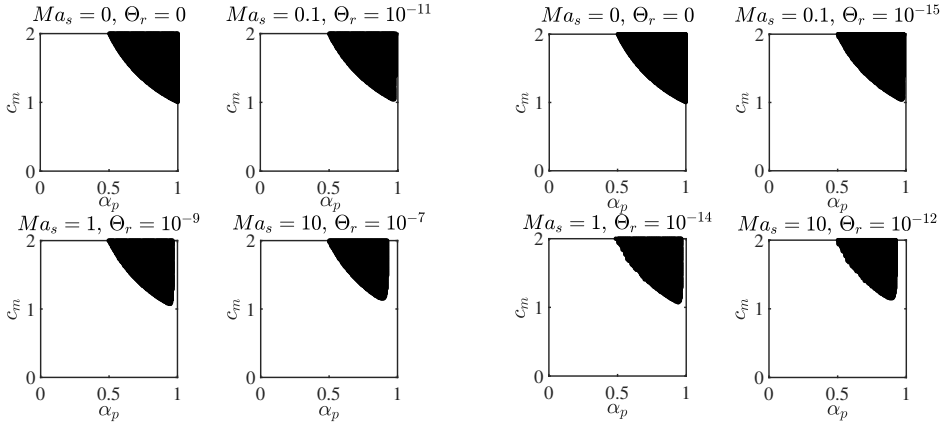

FIGURE 4. Hyperbolicity plot for the full (left) and simplified (right) 1-D model for granular flow ($Z = 0$) with varying Ma_s. The Sturm test function is negative in black regions, which correspond to unphysical values of c_m as discussed in §3.2. The minimum value of Θ_r needed to avoid round-off error is shown.

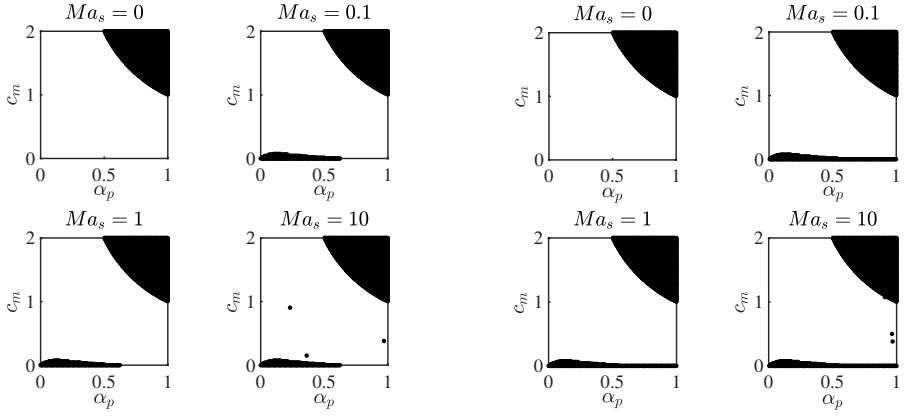

FIGURE 5. Hyperbolicity plot for the full (left) and simplified (right) 1-D model for neutrally buoyant flow ($Z = 1$) and varying Ma_s. The Sturm test function is negative in black regions, indicating that the 1-D model has complex eigenvalues. As shown in the analysis of the Sturm coefficients in §3.2, only the black regions with $c_m < 0.085$ are of interest.

3.3.3. *Bubbly flow with* $\rho_p = 0$

The limit $Z \to \infty$ corresponds to a bubbly flow with $\rho_p = 0$. From the hyperbolicity plot in figure 7, we can again observe that the models are hyperbolic except for a small region near $c_m = 0$. Furthermore, for the simplified model, the non-hyperbolic region is very small and can be easily avoided by proper choices for $c_m^\star$ and τ_a. In figure 6, examples with complex eigenvalues corresponding to small c_m are shown. It can be observed that with $Z = 10000$ the eigenvalues for the two models are nearly identical. In general, as predicted from the hyperbolicity plot in figure 7, the full model has the largest region of parameter space in which it is hyperbolic. As mentioned earlier, the Boltzmann–Enskog fluxes are valid for a hard-sphere mixture, so neglecting them as done in the simplified model may be allowable without significantly changing the hyperbolicity. The added-

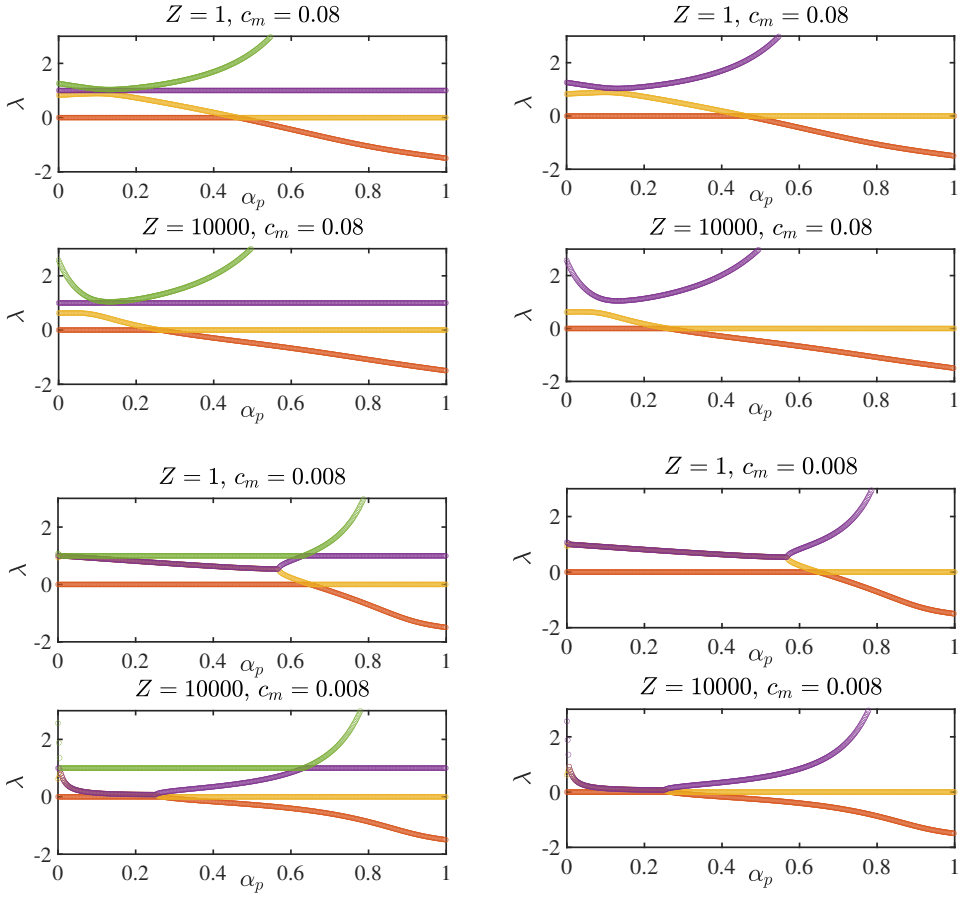

FIGURE 6. Eigenvalues dependent on α_p for the full (left) and simplified (right) 1-D models. Complex eigenvalues are observed in the bottom panels (top: $c_m = 0.08$, bottom: $c_m = 0.008$) and only the real parts are plotted. Both models yield similar eigenvalues. The two eigenvalues that become complex correspond to the particle-phase eigenvalues at $\alpha_p = 0$ in (3.7).

mass contribution to the particle-phase pressure tensor then determines the domain of hyperbolicity of the two-fluid model.

In conclusion, it is worth noting that in the full model the region of hyperbolicity for $0.7 < \alpha_p$ includes $c_m \to 0$. In other words, when the particle-phase volume fraction is near unity, the added mass has no effect on the well-posedness of the full model. Thus, c_m can take any value in the interval $[0, 1]$ for densely packed particles. In general, the effect of added mass on hyperbolicity is most important for $\alpha_p \approx 0.1$, regardless of the material-density ratio.

4. Numerical examples of 1-D model

To illustrate the behaviour of the proposed two-fluid model, in this section we develop a 1-D numerical solver for the full model written in conservative form. In table 5, the 1-D two-fluid model used in the numerical simulations with fluxes (left-hand side) and source terms (right-hand side) is provided in terms of the conserved variables $\mathbf{Y}$. These

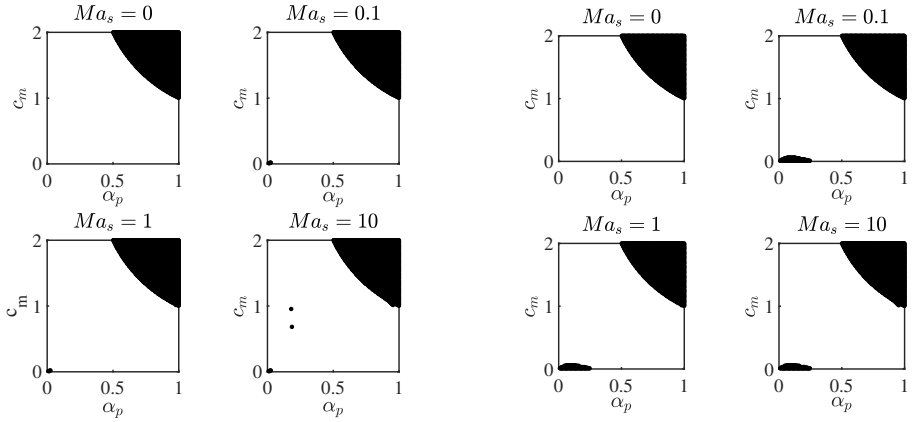

FIGURE 7. Hyperbolicity plot for the full (left) and simplified (right) 1-D model for bubbly flow ($Z \to +\infty$) and varying Ma_s. The Sturm test function is negative in black regions, indicating that the 1-D model has complex eigenvalues. As shown in the analysis of the Sturm coefficients in §3.2, only the black regions with $c_m < 0.085$ are of interest.

variables have been normalized by the constant particle density ρ_p, as are all terms in the model equations.

4.1. *Conservative form of 1-D model*

The added-mass contribution to the particle-phase pressure tensor $\boldsymbol{P}^a_{fp}$ is purely mechanical. This implies that the granular energy balance for Θ_p has a compression source term that depends only on the 'thermodynamic' pressure p_p (see Appendix A in Houim & Oran 2016, for details). Without this property, the source term can generate a negative granular temperature when the thermodynamic pressure is null. Using the 1-D model in table 5, the granular energy balance becomes (with $\gamma_p = 5/3$)

$$\frac{3}{2}\left(Y_2\partial_t\Theta_p + Y_2X_4\partial_x\Theta_p\right) = -p_p\partial_xX_4 - 2\alpha_p^\star\Theta_p[(X_4 - X_5)\partial_xZ - Z\partial_xX_5] + K[2(1-a)X_8 - 3a\Theta_p] + \frac{1}{2}\max(S_a, 0)\left[(X_4 - X_5)^2 - 3\Theta_p\right] \quad (4.1)$$

which has the necessary property that the right-hand side is non-negative when Θ_p is null. In contrast, if p_p were replaced by $(p_p + P^a_{fp})$ in (4.1), then the first term on the right-hand side would be negative when $\Theta_p = 0$ and ∂_xX_4 is positive (i.e., during expansion of the particle phase), leading to a non-physical negative granular temperature. Finally, note that body forces (i.e. gravity) do not appear in (4.1) and, therefore, it can be solved in place of the total energy balance to avoid the associated numerical errors observed in §4.3.

The mixture mass ($\varrho = Y_2 + Y_3$), momentum $\mathcal{M} = Y_4 + Y_5$ and energy $\mathcal{E} = Y_6 + Y_7$ balances can be written as

$$\begin{aligned} \partial_t\varrho + \partial_x\mathcal{M} &= 0 \\ \partial_t\mathcal{M} + \partial_x(Y_4X_4 + Y_5X_5 + P_f + p_p + \alpha_p^\star ZR) &= \varrho g_x \\ \partial_t\mathcal{E} + \partial_x(Y_6X_4 + Y_7X_5 + \alpha_f^\star P_fX_5 + \alpha_p^\star P_fX_4 + p_pX_4 + \alpha_p^\star ZRX_4 + r) &= \mathcal{M}g_x \end{aligned} \quad (4.2)$$

which have the form of hyperbolic conservation laws, albeit with rather complex momentum and energy fluxes. From a computational standpoint, (4.2) can be solved with the

$$\partial_t Y_1 + \partial_x(Y_1 X_4) = 0$$
$$\partial_t Y_2 + \partial_x Y_4 = S_a$$
$$\partial_t Y_3 + \partial_x Y_5 = -S_a$$
$$\partial_t Y_4 + \partial_x(Y_4 X_4 + p_p) = Y_2 g_x - \partial_x(\alpha_a P^a_{fp}) - \alpha^\star_p \partial_x P_f - F_{pf} + K(X_5 - X_4) + S_{fp}$$
$$\partial_t Y_5 + \partial_x(Y_5 X_5 + P_f + \alpha^\star_p Z R) = Y_3 g_x + \partial_x(\alpha_a P^a_{fp}) + \alpha^\star_p \partial_x P_f + F_{pf} + K(X_4 - X_5) - S_{fp}$$
$$\partial_t Y_6 + \partial_x(Y_6 X_4 + p_p X_4) = Y_4 g_x - X_4 \partial_x(\alpha_a P^a_{fp}) - X_4 \alpha^\star_p \partial_x P_f - D_{pf} - D_E + S_E$$
$$\partial_t Y_7 + \partial_x(Y_7 X_5 + \alpha^\star_f P_f X_5 + \alpha^\star_p P_f X_4 + \alpha^\star_p Z R X_4 + r) = Y_5 g_x + X_4 \partial_x(\alpha_a P^a_{fp}) + X_4 \alpha^\star_p \partial_x P_f + D_{pf} + D_E - S_E$$
$$\partial_t Y_8 + \partial_x(Y_8 X_5) = D_{PT} - X_1 \varepsilon_{PT} - 2 X_3 X_8 \partial_x X_5$$

where the conserved variables are

$$\rho_p \mathbf{Y} = (\rho_p \alpha_p, \rho_e \alpha^\star_p, \rho_f \alpha^\star_f, \rho_e \alpha^\star_p u_p, \rho_f \alpha^\star_f u_f, \rho_e \alpha^\star_p E_p, \rho_f \alpha^\star_f E_f, \rho_f \alpha^\star_f k_f)^t$$

and the primitive variables are $\mathbf{X} = (Y_1, Y_2, Y_3, Y_4/Y_2, Y_5/Y_3, Y_6/Y_2, Y_7/Y_3, Y_8/Y_3)^t$. The other model parameters are as follows:

$$\alpha_p = X_1 \qquad \alpha_f = 1 - \alpha_p \qquad Z = \frac{X_2 + X_3 - X_1}{\alpha_f} \qquad g_0 = \frac{1 + \alpha_f}{2\alpha_f^3}$$

$$\alpha^\star_f = \frac{X_3}{Z} \qquad \alpha^\star_p = 1 - \alpha^\star_f \qquad \alpha_a = \alpha^\star_p - \alpha_p = c_m \alpha_f \alpha_p \qquad \frac{\rho_e}{\rho_p} = \frac{\alpha_p + Z\alpha_a}{\alpha^\star_p}$$

$$S_a = \frac{1}{\tau_a} Z \alpha_f \alpha_p (c^\star_m - c_m) \qquad S_{fp} = \max(S_a, 0) X_5 + \min(S_a, 0) X_4$$

$$\tau_a = \frac{4 d_p^2 \alpha^\star_f}{3 \nu_f C_D Re_p \alpha_f} \qquad S_E = \max(S_a, 0) \left(\frac{1}{2} X_5^2 + X_8 \right) + \min(S_a, 0) X_6$$

$$P_f = p_f + 2 Z X_8 \qquad R = \Theta_p + \frac{1}{\gamma_p} (X_4 - X_5)^2 \qquad r = 2 Z \alpha^\star_p \Theta_p (X_4 - X_5)$$

$$F_{pf} = \alpha^\star_p R \partial_x Z + (\gamma_p - 1) \alpha^\star_p Z (X_5 - X_4) \partial_x X_5 \qquad D_{pf} = X_4 F_{pf} + 2 \alpha^\star_p \Theta_p [(X_4 - X_5) \partial_x Z - Z \partial_x X_5]$$

$$\Theta_f = (\gamma_f - 1) \left(X_7 - \frac{1}{2} X_5^2 - X_8 \right) \qquad p_f = Z \Theta_f - \gamma_f (\gamma_f - 1) Z_0 p^\star_o \frac{\alpha_f}{\alpha^\star_f}$$

$$\Theta_p = (\gamma_p - 1) \left(X_6 - \frac{1}{2} X_4^2 \right) \qquad p_p = (\alpha_p + Z\alpha_a) \Theta_p (1 + 4 \alpha^\star_p g_0)$$

$$P^a_{fp} = \frac{1}{\gamma_p} Z (X_4 - X_5)^2 (1 + 4 \alpha^\star_p g_0) \qquad \tau_p = \frac{d_p^2}{Z \nu_f} \qquad Re_p = \frac{d_p |X_4 - X_5|}{\nu_f}$$

$$K = \frac{3 \alpha^\star_p C_D Re_p}{4 \tau_p} \qquad a = \frac{1 + Z \alpha_p \alpha_f}{1 + 1.73 Z \alpha_p \alpha_f} \qquad D_E = K \left[X_4 (X_4 - X_5) + 3 a \Theta_p - 2(1 - a) X_8 \right]$$

$$D_{PT} = K \left[(X_4 - X_5)^2 + 3 a \Theta_p - 2(1 - a) X_8 \right] \qquad \varepsilon_{PT} = \frac{C_f}{d_p} X_8^{3/2} \qquad c^\star_m = \frac{1}{2} \min(1 + 2\alpha_p, 2)$$

TABLE 5. One-dimensional compressible two-fluid model in conservative form with densities and pressures normalized by the particle material density ρ_p. The terms of the left-hand side are the conservative fluxes, while those on the right are interphase exchange terms and g_x is the component of gravity in the x direction. The fluid kinematic viscosity is ν_f and the particle diameter is d_p. For water, $\nu_f = 10^{-6}$ m^2/s and the stiffened-gas-model parameters are $\gamma_f = 29/4$ and $p^\star_o = 10^8$ m^2/s^2. Z_0 is the reference density ratio and $C_f = 1$. For the particle phase, $\gamma_p = 5/3$ and C_D is the Re_p-dependent drag coefficient where, for Stokes drag, $C_D Re_p = 24$.

PTKE and particle-phase balances:

$$\begin{aligned}
\partial_t Y_1 + \partial_x(Y_1 X_4) &= 0 \\
\partial_t Y_2 + \partial_x Y_4 &= S_a \\
\partial_t Y_4 + \partial_x(Y_4 X_4 + p_p) &= Y_2 g_x - \partial_x(\alpha_a P^a_{fp}) - \alpha^\star_p \partial_x P_f - F_{pf} + K(X_5 - X_4) - S_{pf} \\
\partial_t Y_6 + \partial_x(Y_6 X_4 + p_p X_4) &= Y_4 g_x - X_4 \partial_x(\alpha_a P^a_{fp}) - X_4 \alpha^\star_p \partial_x P_f - D_{pf} - D_E - S_E \\
\partial_t Y_8 + \partial_x(Y_8 X_5) &= -2 X_3 X_8 \partial_x X_5 + D_{PT} - X_3 \varepsilon_{PT}
\end{aligned} \tag{4.3}$$

using operator splitting for the left/right-hand sides, respectively. Here, the left-hand sides are fluxes in the finite-volume sense, whereas the right-hand sides are source terms. Alternatively, the balance for Y_6 can be replaced with the granular energy balance for Θ_p shown in (4.1), which is preferable for dissipative systems to avoid round-off errors due to the very small value of Θ_p (see Houim & Oran 2016, for a discussion of this point), and for the numerical treatment of body forces.

4.2. *Numerical solver*

The 1-D model in table 5 has the form

$$\partial_t \mathbf{Y} + \partial_x \boldsymbol{f}(\mathbf{Y}) = \boldsymbol{h}(\mathbf{Y}) \tag{4.4}$$

where $\boldsymbol{f}$ are the spatial fluxes, and $\boldsymbol{h}$ are the source terms. In the numerical solver for (4.4), the conservative variables in each grid cell are updated using an explicit algorithm:

$$\mathbf{Y}^{n+1}_i = \mathbf{Y}^n_i - \frac{\Delta t}{\Delta x}(\boldsymbol{f}^n_i - \boldsymbol{f}^n_{i-1}) + \Delta t\, \boldsymbol{h}(\mathbf{Y}^n_{i+1}, \mathbf{Y}^n_i, \mathbf{Y}^n_{i-1}). \tag{4.5}$$

The source term in (4.5) is evaluated using a central-difference formula for the spatial gradient. In principle, the source term could be stiff and one might want to use an implicit solver. However, we found that the time step required for the spatial fluxes is small enough that this is unnecessary. We should note that for simulations starting with zero particle-phase energy, the explicit Euler scheme for the gravity term generates a negative granular temperature (i.e. $Y^0_4 = Y^0_6 = 0$ yields $Y^1_4 = \Delta t Y^0_2 g_x$, $Y^1_6 = 0$). In general, if there is mean slip between the phases (i.e., $Z_0 \neq 1$), the granular temperature becomes positive everywhere in the domain after a few time steps. To avoid such numerical issues, when evaluating the particle pressure and spatial fluxes, the granular temperature is set to zero whenever it is negative.

The numerical fluxes in (4.5) are defined using a classical HLL approach (Harten *et al.* 1983; Toro 1997):

$$\boldsymbol{f}^n_i = \frac{a^+ \boldsymbol{f}(\mathbf{Y}^n_i) - a^- \boldsymbol{f}(\mathbf{Y}^n_{i+1}) + a^+ a^- (\mathbf{Y}^n_{i+1} - \mathbf{Y}^n_i)}{a^+ - a^-} \tag{4.6}$$

where $a^- < 0 < a^+$ correspond to the minimum and maximum eigenvalues of the system. In all cases considered below, these eigenvalues come from the stiffened-gas model and $a^- \approx -a^+$. In our simulations, the eigenvalues are computed at each time step from the characteristic polynomial. On a uniform grid with spacing Δx, the time step is set using $\Delta x/\Delta t = 2\max(a^+, -a^-)$. As described in §3, the six other eigenvalues of the 1-D system are order one in magnitude, and thus are at least two orders of magnitude smaller than a^+. As a consequence, the HLL fluxes in (4.6), designed for two-wave systems (Toro 1997), will generate significant numerical diffusion for the system in table 5. For example, the effective diffusivity of the volume fraction is $D \propto \Delta x\, a^+$ due to the final difference term on the right-hand side of (4.6). For this reason, unless Δx is very small, the material

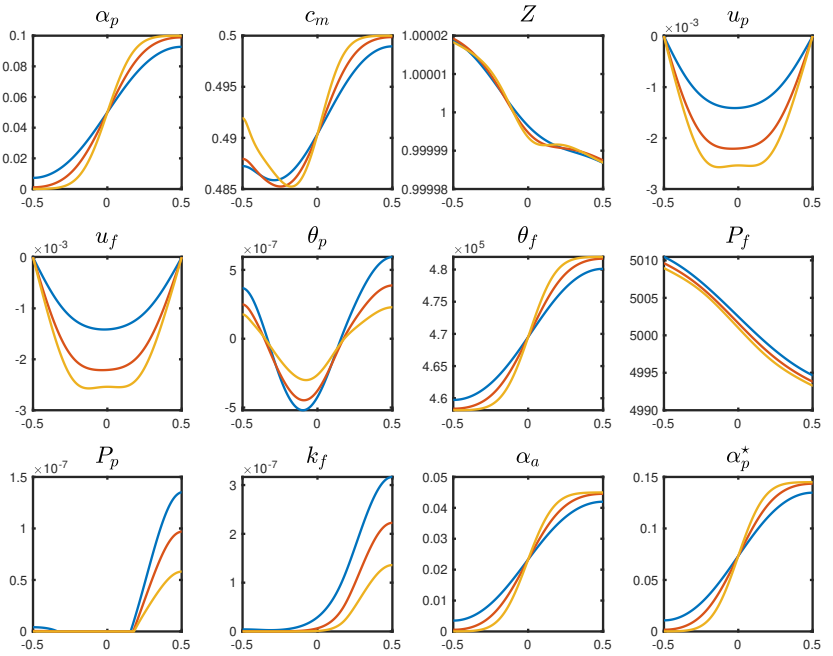

FIGURE 8. Primitive variables at $t = 0.1$ s for Riemann problem with $Z_0 = 1$ and $\Delta x = 1/N$ m (blue: $N = 1000$, red: $N = 2000$, gold: $N = 4000$). The exact solution for α_p is a step function at $x = 0$. Here, the HLL fluxes result in numerical diffusion of the volume fractions, which can be reduced by increasing N.

interface for the density-matched case ($Z_0 = 1$), for which the mean velocity is very small, will be smeared out over time. Future work should therefore focus on developing hyperbolic solvers specifically for multiphase systems to reduce the numerical diffusion using higher-order spatial reconstruction schemes (Toro 1997).

4.3. *Numerical examples*

The numerical examples provided in this section illustrate the behaviour of the model for Riemann problems with different initial conditions on the right/left sides of the domain. In all cases, the initial value $Z = Z_0$ is used (i.e. fixed material-density ratio) and corresponds to monodisperse particles in a given fluid with kinematic viscosity $\nu_f = 10^{-6}$ m^2/s. The fluid temperature Θ_f is set to be 5000 m^2/s^2 larger than Θ_0 in the stiffened-gas model. For simplicity, we consider Stokes drag ($C_D Re_p = 24$), a particle diameter of $d_p = 10^{-3}$ m, and set $c_m^\star = 1/2$. Finally, in order to keep the time step reasonable, we set $p_o^\star = 10^4$ m^2/s^2, which yields $a^+ \approx 775$ m/s. Increasing $p_o^\star$ will result in smaller variations in Z, but requires a correspondingly smaller time step. The computational domain is taken as $x \in [-1/2, 1/2]$ m and zero-flux boundary conditions are employed on each end. To illustrate the effect of numerical diffusion in the HLL scheme, the grid spacing is set to $\Delta x = 1/N$ m with $N = (1000, 2000, 4000)$.

In the first example, we consider a case with $Z_0 = 1$. The initial conditions are $\alpha_p = 0$ on the left half and $\alpha_p = 0.1$ on the right half of the domain. The fluid and particle velocities and the granular temperature are null. With gravity, a pressure gradient

develops in the fluid phase and Z becomes very weakly dependent on x. Because the particles have the same density as the fluid, the exact solution for α_p does not change with time. However, as seen in figure 8, the HLL fluxes are diffusive, leading to a smearing out of the material interface. Without gravity, numerical diffusion is also observed for α_p even though the velocities are null. At shorter times (but still long compared to the fluid speed of sound), the numerical diffusion is less obvious. As expected for $Z_0 = 1$, aside from the volume fractions and P_f, the primitive variables are nearly uniform. Note that the particle pressure P_p is very small due to the negligible slip velocity and small Θ_p. For the exact solution, Θ_p is null and, as discussed earlier, negative values are computed due to the treatment of body forces with the Euler time step. Finally, the added-mass c_m remains close to the equilibrium value of 0.5, and thus well above the minimum value required for hyperbolicity.

In the second example, we consider a case with $Z_0 = 10^4$ corresponding to buoyant particles. The initial conditions are again $\alpha_p = 0$ on the left half and $\alpha_p = 0.1$ on the right half of the domain. The fluid and particle velocities and the granular temperature are null. With gravity, a pressure gradient develops in the fluid phase and Z becomes very weakly dependent on x. The buoyancy force makes u_p positive, moving particles towards the top of the domain. However, as seen in figure 9, the HLL fluxes lead to a smearing out of the material interface, with the numerical diffusion resisting the rise velocity. A finer grid exhibits less numerical diffusion, but the smearing of the volume fraction is still obvious. Presumably, if the grid were made fine enough, α_p would remain near zero for $x < 0$, and be larger at $x = 0.5$ due to buoyancy. In general, the primitive variables are non-uniform due to the buoyancy force. The particle pressure P_p is significant due to the slip velocity. As in the first example, the added-mass c_m remains close to the equilibrium value of 0.5, and thus well above the minimum value required for hyperbolicity. A case with $Z_0 = 10^{-4}$ (not shown) exhibits similar behaviour, but with the particle volume fraction larger at the bottom of the domain.

In summary, aside from excessive numerical diffusion due to the HLL fluxes, solutions to the model in table 5 exhibit the expected physical behaviour. Depending on the value of Z_0, the particle pressure can play a significant role in the momentum balances. In real applications, Θ_p (and, hence, p_p) will be much smaller due to inelastic collisions and lubrication effects (Abbas *et al.* 2010). However, this will not affect the hyperbolicity. Furthermore, the added-mass c_m can vary spatially due to transport between regions with different volume fractions, but always remains well above the minimum value of 0.085 needed to ensure hyperbolicity.

5. Discussion and conclusions

The compressible two-fluid model in table 2 describes inviscid fluids with arbitrary material-density ratios. As seen from the examples in the previous sections, the model for $\boldsymbol{P}_p$ plays a key role in the hyperbolicity of the two-fluid model. In particular, when the material-density ratio Z is non-zero, $\boldsymbol{P}_p$ must be non-zero when $\Theta_p = 0$ in order to eliminate complex eigenvalues. Following Batchelor (1988) and Zhang *et al.* (2006), we have thus included an added-mass contribution to the particle-phase pressure tensor that depends on the slip velocity between the phases. For bubbly flow where the particle shape is flexible, the g_0 expression for solid particles is likely to diverge too quickly with increasing α_p. On the other hand, with rigid particles a frictional component must be added to $\boldsymbol{P}_p$, which is independent of Θ_p. Houim & Oran (2016) have analysed such a case and showed that the eigenvalues remain real valued. Therefore, the overall conclusion

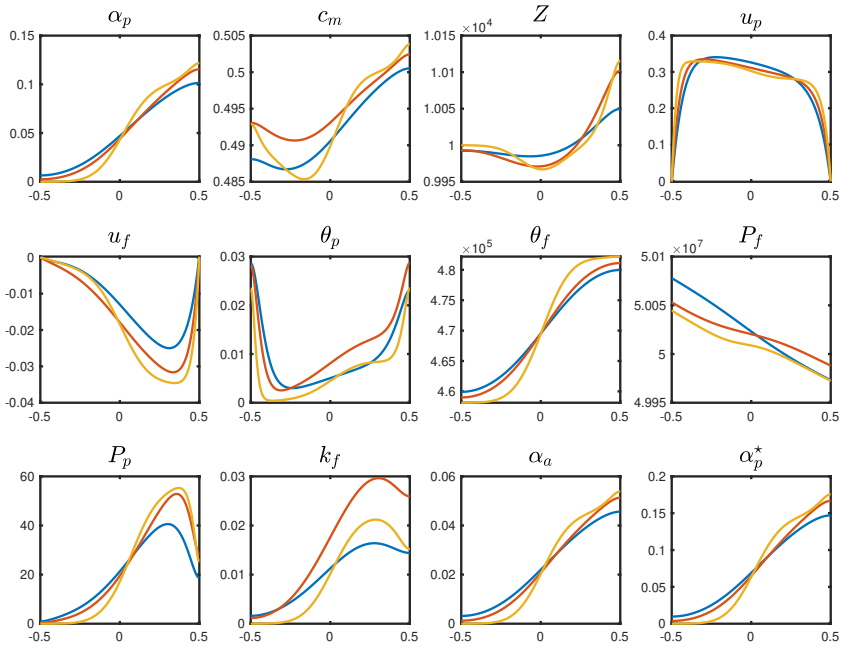

FIGURE 9. Primitive variables at $t = 0.1$ s with $Z_0 = 10^4$ and $\Delta x = 1/N$ m (blue: $N = 1000$, red: $N = 2000$, gold: $N = 4000$). Due to the finer mesh, numerical diffusion is less important for larger N as can be seen from the spatial distribution of α_p.

is that the two-fluid model in table 2 provides a hyperbolic inviscid model for describing compressible disperse-phase flows for all material-density ratios.

5.1. *Extension to viscous flows and other interphase forces*

The model equations in table 2 can be augmented in different directions. First, to model viscous flows (Guazzelli & Pouliquen 2018; Abbas *et al.* 2010), (traceless) viscous stress tensors for the fluid and particle phases can be added to the momentum and energy balances. Note that for the fluid phase, $\boldsymbol{b}$ acts like a pseudo-turbulent viscous stress and can be modelled as a Newtonian fluid with an effective viscosity depending on k_f and ε_{PT}. The parameter a appearing in D_E and D_{PT} determines the distribution of pseudo-turbulent kinetic equation between k_f and Θ_p. The latter has been investigated for spatially homogeneous, incompressible flow by Tavanashad *et al.* (2019) over a wide range of material-density ratios, and these results could be use to develop a correlation for a. Likewise, C_f fixes the value of k_f/u_{fp}^2 and can be fit to the data of Tavanashad *et al.* (2019). As with all two-fluid models, a closure for the drag coefficient K must be provided, which will depend, as usual, on the particle Reynolds number and volume fraction in addition to the fluid Mach number. Finally, additional interphase forces can be added to the momentum and energy balances to describe the effects of mean shear and vorticity on the disperse phase. As mentioned earlier, although these forces contain spatial gradients of the phase velocities, they act normal to the flow direction and, therefore, do not change the hyperbolicity of the system. Note that the effect of "turbulent dispersion" of the disperse phase is already included using the tensor $\boldsymbol{R}_f$, and thus no additional

terms are needed in the balances in table 2. The same is true for the virtual-mass force, which is accounted for as added mass. The coefficient of the lift force in $\boldsymbol{F}_{fp}$ should be revisited to account for surface-tension effects with deformable particles (du Cluzeau *et al.* 2020).

5.2. *Two-fluid model for bubbly flow with constant ρ_f*

For bubbly flow where $\rho_p \ll \rho_f$, the two-fluid model in table 2 can be simplified by removing the transport equation for E_f and treating ρ_f as constant. The fluid pressure is then found using the condition that $\alpha_f^\star + \alpha_p^\star = 1$. This seven-equation model is shown in table 6. It is important to note that while the mean velocity fields are weakly coupled with the pseudo-turbulence kinetic energy, it is often necessary to solve for k_f and Θ_p for other purposes. For example, k_f will be needed to model the effective viscosity or the effective diffusivity of a passive scalar transported by the fluid (Peng *et al.* 2019). As mentioned above, the bubbly-flow model in table 6 can be augmented with a viscous-stress tensor (including pseudo-turbulence) for the fluid phase. Unlike in most other hyperbolic formulations for bubbly flows (see, for example, Panicker *et al.* 2018), it is not necessary to add a turbulent-dispersion term to enforce hyperbolicity. As shown in appendix B, the model for $\boldsymbol{P}_p$ ensures global hyperbolicity. In the terminology of two-fluid models (see Lhuillier *et al.* 2013), the seven-equation two-fluid model in table 6 is a two-pressure model with mixture pressure tensor $\boldsymbol{P} = (p_p + p_f)\boldsymbol{I}$. As we show in appendix B, the shared-pressure model with $\boldsymbol{P}_p = 0$ is not hyperbolic (Drew & Passman 1998) and, thus, cannot be used for bubbly flow simulations because it produces non-physical solutions (see examples in Panicker *et al.* 2018).

5.3. *Relation to effective-field models*

Lhuillier *et al.* (2013) discuss the history of effective-field models for disperse flows, providing insights into why past formulations are mathematically ill-posed. It is therefore of interest to compare the two-fluid model in table 2 to their formulation in order to understand why it is hyperbolic. However, even before performing this exercise, it is noteworthy that these authors suggest that "a promising direction is to associate added-mass and the pseudo-turbulence of the particles". For clarity, in this section we will use the notation developed in this work. However, we should emphasize that as discussed in appendix A the effective-field model is written in terms of the velocity $\boldsymbol{v}_k$, while here we use $\boldsymbol{u}_k$ to account for the added mass.

The pseudo-turbulent kinetic energy in Lhuillier *et al.* (2013) is denoted by K_k, so that $K_f = k_f$ and $K_p = \frac{1}{\gamma_p - 1}\Theta_p$ in our notation. In other words, as the particles have no internal energy, the granular temperature plays the role of the pseudo-turbulent kinetic energy of the particle phase. The momentum balances in Lhuillier *et al.* (2013) are written in our notation as

$$\alpha_p^\star \rho_e \frac{D_p \boldsymbol{u}_p}{Dt} + \partial_{\mathbf{x}} \cdot \boldsymbol{\Pi}_p + \alpha_p^\star \partial_{\mathbf{x}} \cdot \boldsymbol{P}_f = -\boldsymbol{F}, \quad \alpha_f^\star \rho_f \frac{D_f \boldsymbol{u}_f}{Dt} + \partial_{\mathbf{x}} \cdot \boldsymbol{\Pi}_f + \alpha_f^\star \partial_{\mathbf{x}} \cdot \boldsymbol{P}_f = \boldsymbol{F} \quad (5.1)$$

where D_k/Dt is the convected derivative with velocity $\boldsymbol{u}_k$, $\boldsymbol{\Pi}_k$ are the phasic stresses, and $\boldsymbol{F} = K\boldsymbol{u}_{pf}$ is the interphase force (i.e, drag). Comparing with table 2, we observe that $\boldsymbol{\Pi}_p = \boldsymbol{P}_p$ and $\boldsymbol{\Pi}_f = \alpha_p^\star \rho_f \boldsymbol{R} - \alpha_a \boldsymbol{P}_{fp}^a$, and that the kinetic-theory expression for $\boldsymbol{P}_f$ includes the pseudo-turbulent pressure due to $\boldsymbol{R}_f$. However, as shown earlier, the two-fluid model is hyperbolic even with $\boldsymbol{R}_f = \boldsymbol{0}$ for the fluid phase, so the most important term is the added-mass-dependent contribution to $\boldsymbol{\Pi}_p$ and $\boldsymbol{\Pi}_f$ (which can alternatively be treated as part of $\boldsymbol{F}$).

$$\partial_t(\rho_p\alpha_p) + \partial_{\mathbf{x}}\cdot(\rho_p\alpha_p\boldsymbol{u}_p) = 0$$
$$\partial_t(\rho_e\alpha_p^\star) + \partial_{\mathbf{x}}\cdot(\rho_e\alpha_p^\star\boldsymbol{u}_p) = S_a$$
$$\partial_t(\rho_f\alpha_f^\star) + \partial_{\mathbf{x}}\cdot(\rho_f\alpha_f^\star\boldsymbol{u}_f) = -S_a$$

$$\partial_t(\rho_e\alpha_p^\star\boldsymbol{u}_p) + \partial_{\mathbf{x}}\cdot(\rho_e\alpha_p^\star\boldsymbol{u}_p\boldsymbol{u}_p + p_p\boldsymbol{I}) = K\boldsymbol{u}_{fp} - \partial_{\mathbf{x}}\cdot(\alpha_a\boldsymbol{P}_{fp}^a) - \alpha_p^\star\partial_{\mathbf{x}}p_f + \boldsymbol{S}_{fp} + \boldsymbol{F}_{fp} + \rho_e\alpha_p^\star\boldsymbol{g}$$

$$\partial_t(\rho_f\alpha_f^\star\boldsymbol{u}_f) + \partial_{\mathbf{x}}\cdot(\rho_f\alpha_f^\star\boldsymbol{u}_f\boldsymbol{u}_f + p_f\boldsymbol{I}) = K\boldsymbol{u}_{pf} + \partial_{\mathbf{x}}\cdot(\alpha_a\boldsymbol{P}_{fp}^a) + \alpha_p^\star\partial_{\mathbf{x}}p_f + \boldsymbol{S}_{pf} + \boldsymbol{F}_{pf} + \rho_f\alpha_f^\star\boldsymbol{g}$$

$$\partial_t(\rho_e\alpha_p^\star E_p) + \partial_{\mathbf{x}}\cdot(\rho_e\alpha_p^\star E_p\boldsymbol{u}_p + p_p\boldsymbol{u}_p) = -D_E - \boldsymbol{u}_p\cdot(\partial_{\mathbf{x}}\cdot\alpha_a\boldsymbol{P}_{fp}^a) - \alpha_p^\star\boldsymbol{u}_p\cdot\partial_{\mathbf{x}}p_f + S_E + D_{fp} + \rho_e\alpha_p^\star\boldsymbol{u}_p\cdot\boldsymbol{g}$$

$$\partial_t(\rho_f\alpha_f^\star k_f) + \partial_{\mathbf{x}}\cdot(\rho_f\alpha_f^\star k_f\boldsymbol{u}_f) + 2\rho_f\alpha_f^\star k_f\partial_{\mathbf{x}}\cdot\boldsymbol{u}_f = D_{PT} - \rho_f\alpha_f^\star\varepsilon_{PT}$$

where $\alpha_p^\star = 1-\alpha_f^\star$, $\alpha_f = 1-\alpha_p$, $\alpha_a = \alpha_p^\star - \alpha_p = c_m\alpha_f\alpha_p$,

$$\rho_e\alpha_p^\star = \rho_p(\alpha_p + Z\alpha_a) \qquad \boldsymbol{u}_{fp} = -\boldsymbol{u}_{pf} = \boldsymbol{u}_f - \boldsymbol{u}_p \qquad c_m^\star = \frac{1}{2}\min(1+2\alpha_p, 2)$$

$$S_a = \frac{1}{\tau_a}\alpha_f\alpha_p(c_m^\star - c_m) \qquad \boldsymbol{S}_{fp} = -\boldsymbol{S}_{pf} = \max(S_a,0)\boldsymbol{u}_f + \min(S_a,0)\boldsymbol{u}_p$$

$$S_E = \max(S_a,0)\left(\frac{1}{2}u_f^2 + k_f\right) + \min(S_a,0)E_p \qquad \tau_a = \frac{4d_p^2\alpha_f^\star}{3\nu_f C_D Re_p\alpha_f}$$

$$p_p = \rho_e\alpha_p^\star\Theta_p\left(1+4\alpha_p^\star g_0\right) \qquad \boldsymbol{P}_{fp}^a = \frac{2\rho_f}{3\gamma_p}\left(\frac{1}{2}u_{fp}^2\boldsymbol{I} + \boldsymbol{u}_{fp}\otimes\boldsymbol{u}_{fp}\right)\left(1+4\alpha_p^\star g_0\right) \qquad g_0 = \frac{1+\alpha_f}{2\alpha_f^3}$$

$$\boldsymbol{F}_{pf} = -\boldsymbol{F}_{fp} = \rho_f\alpha_p^\star(\gamma_p - 1)\left(tr(\boldsymbol{\Gamma})\boldsymbol{u}_{fp} + \frac{2}{\gamma_p}\boldsymbol{S}\cdot\boldsymbol{u}_{fp}\right) \qquad D_{fp} = \boldsymbol{u}_p\cdot\boldsymbol{F}_{fp} + 2\rho_f\alpha_p^\star\Theta_p\partial_{\mathbf{x}}\cdot\boldsymbol{u}_f$$

$$D_E = K\left[\boldsymbol{u}_p\cdot\boldsymbol{u}_{pf} + 3a\Theta_p - 2(1-a)k_f\right] \qquad D_{PT} = K\left[u_{pf}^2 + 3a\Theta_p - 2(1-a)k_f\right]$$

$$\Theta_p = (\gamma_p - 1)\left(E_p - \frac{1}{2}u_p^2\right) \qquad \varepsilon_{PT} = C_f k_f^{3/2}/d_p$$

$$K = \frac{3\rho_p\alpha_p^\star C_D Re_p}{4\tau_p} \qquad \tau_p = \frac{d_p^2}{Z\nu_f} \qquad a = \frac{1+Z\alpha_a}{1+Z(\alpha_f\alpha_p b + \alpha_a)} \qquad Z = \frac{\rho_f}{\rho_p}$$

TABLE 6. Seven-equation two-fluid model for bubbly flow with constant fluid density and $\gamma_p = 5/3$. C_D is the drag coefficient that depends on the particle Reynolds number and volume fraction, and $\boldsymbol{g}$ is gravity. The energy balance for E_p can be rewritten in terms of Θ_p. In principle, this model can be applied for any value of Z provided ρ_f can be treated as constant (i.e., low-Mach-number flows). In the fluid momentum balance, a traceless stress tensor due to $\boldsymbol{R}$ and $\boldsymbol{R}_f$ can be included without changing the hyperbolicity of the system.

The energy equation for the particle phase found from the balances in table 2 is

$$\alpha_p^\star\rho_e\frac{D_pK_p}{Dt} + p_p\partial_{\mathbf{x}}\cdot\boldsymbol{u}_p = -K[aK_p - (1-a)K_f] \tag{5.2}$$

where the left-hand side is a non-dissipative pseudo-turbulent kinetic energy exchange

term. The parameter a determines the amount of mean kinetic energy that is directly dissipated to fluid-phase internal energy, so for a non-dissipative system $a = 0$. Recalling that $\boldsymbol{b}$ and ε_{PT} arise due to dissipation of fluid-phase pseudo-turbulent kinetic energy to fluid-phase internal energy, the non-dissipative terms in the pseudo-turbulent kinetic energy balance yield

$$\alpha_f^\star \rho_f \frac{D_f K_f}{Dt} + \frac{2}{3}\alpha_f^\star \rho_f K_f \partial_{\mathbf{x}} \cdot \boldsymbol{u}_f + \boldsymbol{u}_{fp} \cdot \boldsymbol{F} = K[aK_p - (1-a)K_f]. \tag{5.3}$$

Then, as could be anticipated from the fact that $\alpha_p^\star \rho_e E_p + \alpha_f^\star \rho_f E_f$ obeys a conservation equation, the sum of (5.2) and (5.3) satisfies the energy conservation condition (2.5) in Lhuillier *et al.* (2013).

Nonetheless, it is important to point out that the trace of $\boldsymbol{P}_p$ is not the inter-facial pressure of the fluid at the particle surface. Indeed, the Θ_p-dependent part of $\boldsymbol{P}_p$ arises in kinetic theory due to particles having different instantaneous velocities. Thus, at best, only the α_a-dependent part of $\boldsymbol{P}_p$ might be assigned to the inter-facial pressure (see Batchelor 1988, for a discussion of the physical reasoning on why this is incorrect). Supporting the arguments made by Lhuillier *et al.* (2013) (and consistent with Batchelor (1988)), taken as a whole these observations suggest that the Θ_p-independent contribution to $\boldsymbol{P}_p$ is a necessary condition for hyperbolicity of two-fluid models.

5.4. *Closing remarks*

Starting from the kinetic-theory-based model derived from first principles in Fox (2019), the definition of the particle mass was extended to include the added mass moving with the velocity of the particle. This resulted in the compressible two-fluid model in table 1. Then, by relaxing the assumption that the pseudo-turbulent kinetic energy in the fluid phase (denoted by $\boldsymbol{R}_f$) attain instantaneously its steady-state value, a transport equation was introduced to model its trace ($2k_f$). The resulting compressible two-fluid model, presented in table 2, has governing equations for pseudo-turbulent kinetic energy in both phases, as well as balance equations for the total energies. The fluid phase is treated as compressible with a stiffened-gas equation of state to describe liquids. As written, the compressible two-fluid model is applicable to flows with an arbitrary material-density ratio $Z = \rho_f/\rho_p$.

While needed for accurate physical modelling (e.g., in gas–particle flows), from the hyperbolicity analysis of the 1-D model it was found that the pseudo-turbulent kinetic energies play no role in determining whether the two-fluid model is hyperbolic. In contrast, g_0 and the particle–fluid–particle stress contribution (i.e., $\alpha_a \boldsymbol{P}_{fp}^a$) to $\boldsymbol{P}_p$ are crucial for obtaining a hyperbolic model for large to intermediate values of Z. Indeed, for $\rho_p = 0$ (mass-less particles), without these contributions the two-fluid model loses hyperbolicity in physically important regions of parameter space (e.g., Θ_p near zero). Future work should therefore focus on obtaining a more fundamental understanding of how to model $\boldsymbol{P}_{fp}^a$ and g_0 in the particle-phase pressure tensor for real physical systems, especially for $Z \approx 1$. To this end, direct-numerical simulations of particle suspensions over a wide range of material-density ratios, Reynolds numbers and volume fractions would be useful (such as is done in Tavanashad *et al.* 2019; Moore & Balachandar 2019; du Cluzeau *et al.* 2020), especially if one can unequivocally relate model variables such as $c_m^\star$ and $\boldsymbol{P}_{fp}^a$ to the data from such simulations (Zhang 2020). Finally, work along the lines of Gu *et al.* (2019) and Abbas *et al.* (2010) will be required to account for viscous effects in the particle phase.

Acknowledgements

This research was partially supported by the MEP department of the Université de Paris–Saclay.

Declaration of Interests

The authors report no conflict of interest.

Appendix A. Relation to virtual-mass force in two-fluid model

Cook & Harlow (1984) derive a two-fluid formulation for the virtual-mass force starting from a three-field model that treats the added mass as a separate field. In their model, the fluid and particle material densities are constant (i.e. the fluid is incompressible), and they assume that $\boldsymbol{u}_p = \boldsymbol{v}_p$. Thus, by using the relation

$$\alpha_f^\star \boldsymbol{u}_f = \alpha_f \boldsymbol{v}_f - \alpha_a \boldsymbol{v}_p, \tag{A 1}$$

the slip velocities are related by

$$\boldsymbol{u}_{fp} = \frac{\alpha_f}{\alpha_f^\star} \boldsymbol{v}_{fp} \tag{A 2}$$

where $\boldsymbol{v}_{fp} = -\boldsymbol{v}_{pf} = \boldsymbol{v}_f - \boldsymbol{v}_p$. For convenience, we define the convected derivative for each phase as

$$\begin{aligned} D_f &= \partial_t + \boldsymbol{v}_f \cdot \partial_{\mathbf{x}}, \\ D_p &= \partial_t + \boldsymbol{v}_p \cdot \partial_{\mathbf{x}}, \end{aligned} \tag{A 3}$$

but will continue to write out the convected derivative for $\boldsymbol{u}_f$. In Cook & Harlow (1984), the mass-exchange source terms involving S_a and the particle pressure p_p are absent. If their method to find the virtual-mass force is employed, these terms will yield non-conservative terms in the mixture model that are unphysical (as defined in Lhuillier *et al.* 2013). Therefore, we will follow their route to the find an expression for the virtual-mass force, but make small modifications to avoid unphysical terms.

In terms of $\boldsymbol{v}_f$ and $\boldsymbol{v}_p$, the mass balances from table 1 yield

$$\partial_t \rho_f \alpha_f + \partial_{\mathbf{x}} \cdot (\rho_f \alpha_f \boldsymbol{v}_f) = 0 \tag{A 4}$$

$$\partial_t \alpha_p + \partial_{\mathbf{x}} \cdot (\alpha_p \boldsymbol{v}_p) = 0 \tag{A 5}$$

$$\partial_t \rho_f \alpha_a + \partial_{\mathbf{x}} \cdot (\rho_f \alpha_a \boldsymbol{v}_p) = S_a \tag{A 6}$$

where $\alpha_f = \alpha_f^\star + \alpha_a$ and $\alpha_a = c_m \alpha_f \alpha_p$. In Cook & Harlow (1984), $\alpha_a = f\alpha_p$ with constant f and ρ_f, which with (A 5) implies that $S_a = 0$ in their three-fluid model. Here, (A 6) is needed to find c_m. However, the time scale τ_a in S_a can be chosen sufficiently small to force $c_m \to c_m^\star$. Nonetheless, in our model the dependence of α_a on α_f is needed to handle the limiting case $\alpha_p \to 1$ and, hence, a constant f can only be used for $\alpha_p \ll 1$. Furthermore, as shown below, the assumption that ρ_f is constant is not required to derive the virtual-mass force.

Using the continuity equations, the momentum balances from table 1 can be rewritten in non-conservative form as

$$\rho_f \alpha_f^\star (\partial_t + \boldsymbol{u}_f \cdot \partial_{\mathbf{x}}) \boldsymbol{u}_f + \alpha_f^\star \partial_{\mathbf{x}} p_f + \partial_{\mathbf{x}} \cdot (\rho_f \alpha_p^\star \boldsymbol{R}) = -\boldsymbol{G}_{fp} + \boldsymbol{S}_{pf} + \boldsymbol{u}_f S_a + \rho_f \alpha_f^\star \boldsymbol{g} \tag{A 7}$$

$$(\rho_f \alpha_a + \rho_p \alpha_p) D_p \boldsymbol{v}_p + \alpha_p^\star \partial_{\mathbf{x}} p_f + \partial_{\mathbf{x}} p_p = \boldsymbol{G}_{fp} + \boldsymbol{S}_{fp} - \boldsymbol{v}_p S_a + (\rho_f \alpha_a + \rho_p \alpha_p) \boldsymbol{g} \tag{A 8}$$

where

$$\boldsymbol{G}_{fp} = \frac{\alpha_f}{\alpha_f^\star} K \boldsymbol{v}_{fp} + \partial_{\mathbf{x}} \cdot (\alpha_a \boldsymbol{P}^a_{fp}) + \boldsymbol{F}_{fp} \tag{A 9}$$

is the interphase momentum-exchange vector. Unlike in Cook & Harlow (1984), we do not have a model for the added-mass momentum; however, from their study we know that the virtual-mass force arises from the shared pressure. Thus, treating the shared pressure as a separate term, we propose a model for the added-mass momentum of the form:

$$\rho_f \alpha_a D_p \boldsymbol{v}_p + (\alpha_v + \alpha_a) \partial_{\mathbf{x}} p_f = -\boldsymbol{G}_a + \boldsymbol{S}_{fp} - \boldsymbol{v}_p S_a + \rho_f \alpha_a \boldsymbol{g}. \tag{A 10}$$

The added-mass pressure coefficient α_v and the force vector $\boldsymbol{G}_a$ are unknown at this point. However, $\boldsymbol{G}_a$ is independent of the shared pressure and is zero when the particles do not move relative to the fluid (i.e., $\boldsymbol{v}_{fp} = 0$ and $\Theta_p = 0$).

Adding and subtracting (A 10) from (A 7) and (A 8), respectively, yields the fluid-phase momentum balance:

$$\rho_f \alpha_f^\star (\partial_t + \boldsymbol{u}_f \cdot \partial_{\mathbf{x}}) \boldsymbol{u}_f + \rho_f \alpha_a D_p \boldsymbol{v}_p + (\alpha_f + \alpha_v) \partial_{\mathbf{x}} p_f = -\boldsymbol{G}_{fp} - \boldsymbol{G}_a + \frac{\alpha_f}{\alpha_f^\star} \boldsymbol{v}_{fp} S_a + \rho_f \alpha_f \boldsymbol{g}, \tag{A 11}$$

and the particle-phase momentum balance:

$$\rho_p \alpha_p D_p \boldsymbol{v}_p + (\alpha_p - \alpha_v) \partial_{\mathbf{x}} p_f + \partial_{\mathbf{x}} p_p = \boldsymbol{G}_{fp} + \boldsymbol{G}_a + \rho_p \alpha_p \boldsymbol{g}. \tag{A 12}$$

As noted by Cook & Harlow (1984), (A 12) is not in the usual form of a two-fluid model due to the incorrrect coefficient for the Archimedes force. Indeed, just as in their work, we shall see that the choice of α_v determines the virtual-mass force.

The next step is to eliminate $\boldsymbol{u}_f$ and $D_p \boldsymbol{v}_p$ from (A 11), using the definition of $\boldsymbol{u}_f$ in (A 1). For this step, two intermediate results are first found from (A 1) and the continuity equations:

$$\begin{aligned} &\rho_f \alpha_f^\star \partial_t \boldsymbol{u}_f = \\ &\quad \rho_f \alpha_f \partial_t \boldsymbol{v}_f - \rho_f \alpha_a \partial_t \boldsymbol{v}_p - \frac{\alpha_f \partial_{\mathbf{x}} \cdot (\rho_f \alpha_a \boldsymbol{v}_p) - \alpha_a \partial_{\mathbf{x}} \cdot (\rho_f \alpha_f \boldsymbol{v}_f)}{\alpha_f^\star} \boldsymbol{v}_{fp} + \frac{\alpha_f}{\alpha_f^\star} \boldsymbol{v}_{fp} S_a \end{aligned} \tag{A 13}$$

and

$$(\alpha_f^\star)^2 \boldsymbol{u}_f \cdot \partial_{\mathbf{x}} \boldsymbol{u}_f = (\alpha_f \boldsymbol{v}_f - \alpha_a \boldsymbol{v}_p) \cdot \left(\alpha_f \partial_{\mathbf{x}} \boldsymbol{v}_f - \alpha_a \partial_{\mathbf{x}} \boldsymbol{v}_p + \frac{\alpha_f \partial_{\mathbf{x}} \alpha_a - \alpha_a \partial_{\mathbf{x}} \alpha_f}{\alpha_f^\star} \boldsymbol{v}_{fp} \right). \tag{A 14}$$

It is noteworthy that (A 13) has the mass-exchange source term coming from the mass balance in (A 6). Combining these two results then provides the expression for the convected derivative of $\boldsymbol{u}_f$ in terms of $\boldsymbol{v}_f$ and $\boldsymbol{v}_p$:

$$\rho_f \alpha_f^\star (\partial_t + \boldsymbol{u}_f \cdot \partial_{\mathbf{x}}) \boldsymbol{u}_f = \rho_f \alpha_f D_f \boldsymbol{v}_f - \rho_f \alpha_a D_p \boldsymbol{v}_p + \frac{\alpha_f}{\alpha_f^\star} \boldsymbol{v}_{fp} S_a + \partial_{\mathbf{x}} \cdot \boldsymbol{P}_{vm}. \tag{A 15}$$

The virtual-mass pressure tensor in (A 15) is defined by

$$\boldsymbol{P}_{vm} = \rho_f \alpha_a \frac{\alpha_f}{\alpha_f^\star} \boldsymbol{v}_{fp} \otimes \boldsymbol{v}_{fp} \tag{A 16}$$

and is the same as in Cook & Harlow (1984). Note that $\boldsymbol{P}_{vm}$ has the same tensorial form as $\boldsymbol{R}$ and, hence, as done below these two tensors can be combined in the fluid-phase momentum balance.

Inserting (A 15) into (A 11), we then find the fluid-phase momentum balance in terms of the two-fluid model variables:

$$\rho_f \alpha_f D_f \boldsymbol{v}_f + (\alpha_f + \alpha_v)\partial_{\mathbf{x}} p_f + \partial_{\mathbf{x}} \cdot \boldsymbol{P}^{\star}_{vm} = -\boldsymbol{G}_{fp} - \boldsymbol{G}_a + \rho_f \alpha_f \boldsymbol{g} \tag{A 17}$$

where $\boldsymbol{P}^{\star}_{vm} = \rho_f \alpha^{\star}_p \boldsymbol{R} + \boldsymbol{P}_{vm}$. The term involving $\boldsymbol{P}_{vm}$ ensures that the two-fluid model is objective in the sense of Drew *et al.* (1979). As expected, (A 17) has no mass-exchange source term and the mixture model found by summing it with (A 12) is conservative. Physically, the pressure tensor (A 16) arises due to the added mass having a different velocity than the bulk fluid, and thus will not be negligible unless $\rho_f \ll \rho_p$. Note that the mixture momentum balance has a virtual-mass pressure contribution of $\partial_{\mathbf{x}} \cdot \boldsymbol{P}^{\star}_{vm}$, which increases the pressure in the direction of the mean-slip velocity. In a constant-density flow, this pressure can be combined with p_f in the fluid momentum equation. The remaining contribution (i.e. that appearing in the particle-phase momentum balance) can be combined with the virtual-mass force.

The momentum balances in (A 12) and (A 17) have the same forms as in Cook & Harlow (1984). We can therefore proceed in the same manner to find an expression for the virtual-mass force. However, to simplify the notation and make the manipulations as transparent as possible, we rewrite the momentum balances as

$$\rho_p \alpha_p D_p \boldsymbol{v}_p + \alpha_p \partial_{\mathbf{x}} p_f - \alpha_v \partial_{\mathbf{x}} p_f = \boldsymbol{G}_p + \rho_p \alpha_p \boldsymbol{g} \tag{A 18}$$

$$\rho_f \alpha_f D_f \boldsymbol{v}_f + \alpha_f \partial_{\mathbf{x}} p_f + \alpha_v \partial_{\mathbf{x}} p_f = \boldsymbol{G}_f + \rho_f \alpha_f \boldsymbol{g} \tag{A 19}$$

where $\boldsymbol{G}_p = \boldsymbol{G}_{fp} + \boldsymbol{G}_a - \partial_{\mathbf{x}} p_p$ and $\boldsymbol{G}_f = -\boldsymbol{G}_{fp} - \boldsymbol{G}_a - \partial_{\mathbf{x}} \cdot \boldsymbol{P}^{\star}_{vm}$. The added-mass force on the particle phase is $\boldsymbol{F}_a = \alpha_v \partial_{\mathbf{x}} p_f$. In constant-density flows, the fluid pressure is fixed by the constraint $\alpha_p + \alpha_f = 1$, which forces the mixture velocity to be divergence free. Thus, the added-mass force is mainly determined by the choice of α_v and $\boldsymbol{G}_a$.

The next step is to find an expression for $\partial_{\mathbf{x}} p_f$ that does not depend on $\boldsymbol{g}$ by taking a linear combination of (A 18) and (A 19). Multiplying the result by α_v provides the definition of the added-mass force:

$$\boldsymbol{F}_a = \alpha_v \frac{\rho_f \alpha_f \boldsymbol{G}_p - \rho_p \alpha_p \boldsymbol{G}_f + \rho_p \rho_f \alpha_p \alpha_f (D_f \boldsymbol{v}_f - D_p \boldsymbol{v}_p)}{\rho_f \alpha_f (\alpha_p - \alpha_v) - \rho_p \alpha_p (\alpha_f + \alpha_v)}. \tag{A 20}$$

If the added-mass force were to depend neither on $\boldsymbol{G}_p$ nor on $\boldsymbol{G}_f$, then we would have to define $\boldsymbol{G}_a$ such that $\rho_f \alpha_f \boldsymbol{G}_p = \rho_p \alpha_p \boldsymbol{G}_f$. However, such a choice makes $\boldsymbol{G}_a$ independent of α_a and is inconsistent with Cook & Harlow (1984). For consistency, one must choose α_v such the coefficient of the convected velocity difference is the same as in (A 16), i.e.,

$$\frac{\alpha_v \rho_p \rho_f \alpha_p \alpha_f}{\rho_f \alpha_f (\alpha_p - \alpha_v) - \rho_p \alpha_p (\alpha_f + \alpha_v)} = \rho_f \alpha_a \frac{\alpha_f}{\alpha^{\star}_f}, \tag{A 21}$$

which yields (as found after equation [19] in Cook & Harlow (1984))

$$\alpha_v = \alpha_a \alpha_p \left(\frac{\rho_f - \rho_p}{\rho_p \alpha_p + \rho_f \alpha_a} \right) = \alpha_a \frac{\alpha_p}{\alpha^{\star}_p} \frac{(\rho_f - \rho_p)}{\rho_e} \tag{A 22}$$

and

$$\boldsymbol{F}_a = \rho_f \alpha_a \frac{\alpha_f}{\alpha^{\star}_f} (D_f \boldsymbol{v}_f - D_p \boldsymbol{v}_p) + \rho_f \alpha_a \frac{\alpha_f}{\alpha^{\star}_f} \left(\frac{\boldsymbol{G}_p}{\rho_p \alpha_p} - \frac{\boldsymbol{G}_f}{\rho_f \alpha_f} \right). \tag{A 23}$$

The first term on the right-hand side is the usual virtual-mass force in two-fluid models, i.e.,

$$\boldsymbol{F}_{vm} = \rho_f \alpha_a \frac{\alpha_f}{\alpha^{\star}_f} (D_p \boldsymbol{v}_p - D_f \boldsymbol{v}_f). \tag{A 24}$$

The second term modifies $\boldsymbol{G}_p$ and $\boldsymbol{G}_f$ in the momentum balances, and can be used to determine $\boldsymbol{G}_a$. It is interesting to note that the pressure coefficient from (A 22) depends on the material-density difference, and changes sign at $\rho_f = \rho_p$. Replacing α_a by $c_m \alpha_f \alpha_p$, the usual virtual-mass constant in (A 24) is $C_a = c_m \alpha_f^2 / \alpha_f^\star$ so that in the limit $\alpha_f = 1$, the standard value of $C_a = c_m = 1/2$ (Milne-Thomson 1968).

The final step is to determine a form for $\boldsymbol{G}_a$. In Cook & Harlow (1984), the particle pressure and $\boldsymbol{R}$ are null and the two-fluid momentum balances have the form

$$\rho_f \alpha_f D_f \boldsymbol{v}_f + \alpha_f \partial_{\mathbf{x}} p_f + \frac{\alpha_f}{\alpha_f^\star} \partial_{\mathbf{x}} \cdot \boldsymbol{P}_{vm} = -\frac{\alpha_f}{\alpha_f^\star} \boldsymbol{G}_{fp} + \boldsymbol{F}_{vm} + \rho_f \alpha_f \boldsymbol{g} \tag{A 25}$$

$$\rho_p \alpha_p D_p \boldsymbol{v}_p + \alpha_p \partial_{\mathbf{x}} p_f - \frac{\alpha_a}{\alpha_f^\star} \partial_{\mathbf{x}} \cdot \boldsymbol{P}_{vm} = \frac{\alpha_f}{\alpha_f^\star} \boldsymbol{G}_{fp} - \boldsymbol{F}_{vm} + \rho_p \alpha_p \boldsymbol{g} \tag{A 26}$$

which can be compared to the ones found above:

$$\rho_f \alpha_f D_f \boldsymbol{v}_f + \alpha_f \partial_{\mathbf{x}} p_f + \frac{\rho_f \alpha_a}{\rho_e \alpha_p^\star} \partial_{\mathbf{x}} p_p + \frac{\alpha_f}{\alpha_f^\star} \partial_{\mathbf{x}} \cdot \boldsymbol{P}_{vm}^\star = -\frac{\alpha_f}{\alpha_f^\star} \boldsymbol{F} + \boldsymbol{F}_{vm} + \rho_f \alpha_f \boldsymbol{g} \tag{A 27}$$

$$\rho_p \alpha_p D_p \boldsymbol{v}_p + \alpha_p \partial_{\mathbf{x}} p_f + \frac{\rho_p \alpha_p}{\rho_e \alpha_p^\star} \partial_{\mathbf{x}} p_p - \frac{\alpha_a}{\alpha_f^\star} \partial_{\mathbf{x}} \cdot \boldsymbol{P}_{vm}^\star = \frac{\alpha_f}{\alpha_f^\star} \boldsymbol{F} - \boldsymbol{F}_{vm} + \rho_p \alpha_p \boldsymbol{g} \tag{A 28}$$

where the exchange force $\boldsymbol{F}$ is defined by

$$\boldsymbol{F} = \frac{\rho_e \alpha_p^\star}{\rho_p \alpha_p} (\boldsymbol{G}_{fp} + \boldsymbol{G}_a) - \frac{\rho_f \alpha_a}{\rho_e \alpha_p^\star} \left(\frac{\rho_e \alpha_p^\star}{\rho_p \alpha_p} + \frac{\alpha_f^\star}{\alpha_f} \right) \partial_{\mathbf{x}} p_p. \tag{A 29}$$

In order for (A 27) to agree with (A 25) when $\boldsymbol{R}$ is null, we must have

$$\boldsymbol{F} = \boldsymbol{G}_{fp} - \frac{\alpha_f^\star}{\alpha_f} \frac{\rho_f \alpha_a}{\rho_e \alpha_p^\star} \partial_{\mathbf{x}} p_p, \tag{A 30}$$

and, hence,

$$\boldsymbol{G}_a = \frac{\rho_f \alpha_a}{\rho_e \alpha_p^\star} (\partial_{\mathbf{x}} p_p - \boldsymbol{G}_{fp}) \tag{A 31}$$

where the pre-factor is the ratio of the added mass to the mass moving with velocity $\boldsymbol{v}_p$. The momentum balances for the two-fluid model in terms of $\boldsymbol{v}_f$ and $\boldsymbol{v}_p$ are thus

$$\rho_f \alpha_f D_f \boldsymbol{v}_f + \alpha_f \partial_{\mathbf{x}} p_f + \frac{\alpha_f}{\alpha_f^\star} \partial_{\mathbf{x}} \cdot \boldsymbol{P}_{vm}^\star = -\frac{\alpha_f}{\alpha_f^\star} \boldsymbol{G}_{fp} + \boldsymbol{F}_{vm} + \rho_f \alpha_f \boldsymbol{g} \tag{A 32}$$

$$\rho_p \alpha_p D_p \boldsymbol{v}_p + \alpha_p \partial_{\mathbf{x}} p_f + \partial_{\mathbf{x}} p_p - \frac{\alpha_a}{\alpha_f^\star} \partial_{\mathbf{x}} \cdot \boldsymbol{P}_{vm}^\star = \frac{\alpha_f}{\alpha_f^\star} \boldsymbol{G}_{fp} - \boldsymbol{F}_{vm} + \rho_p \alpha_p \boldsymbol{g} \tag{A 33}$$

where $\boldsymbol{G}_{fp}$ is given in (A 9). From a numerical perspective, the two-fluid model in table 1 should be preferable because it is not necessary to approximate $\boldsymbol{F}_{vm}$ numerically.

To conclude, it is interesting to note that the fluid drag in (A 9) depends on the added mass (see Osnes *et al.* 2019, for a discussion of this issue for compressible flow). For example, with $\alpha_a = \frac{1}{2} \alpha_f \alpha_p$ the drag coefficient increases like $1/\alpha_f^2$ with decreasing α_f, which is reminiscent of the drag law of Richardson & Zaki (1954) (see, also Kramer *et al.* 2019). Inversely, the dependence of the drag coefficient on α_f may be interpreted as resulting from the added volume α_a. It would therefore be interesting to explore the connection between added mass and the drag law using particle-resolved direct-numerical-simulation data with a model for the velocity wake (see, e.g., Moore & Balachandar 2019).

Appendix B. Hyperbolicity of the incompressible bubbly flow model

In this appendix, we investigate the hyperbolicity of the incompressible bubbly flow model in table 6. Here, we consider the limit case $Z \to +\infty$. Following the method described in Panicker *et al.* (2018) (see also Drew & Passman 1998), the independent variables are $\mathbf{X} = (\alpha_a, \alpha_f^\star, p_f/\rho_f, u_p, u_f, E_p)^t$. The variable k_f does not affect the fluxes of the other variables and its balance equation has a real eigenvalue equal to u_f. The remaining six equations in the 1-D model without source terms are then

$$\begin{gathered}
\partial_t \alpha_p + X_4 \partial_x \alpha_p + \alpha_p \partial_x X_4 = 0 \\
\partial_t X_1 + X_4 \partial_x X_1 + X_1 \partial_x X_4 = 0 \\
\partial_t X_2 + X_5 \partial_x X_2 + X_2 \partial_x X_5 = 0 \\
X_1 \partial_t X_4 + X_1 X_4 \partial_x X_4 + \partial_x P_p + \alpha_p^\star \partial_x X_3 + F'_{pf} \partial_x X_5 = 0 \\
X_2 \partial_t X_5 + X_2 X_5 \partial_x X_5 + X_2 \partial_{\mathbf{x}} X_3 - \partial_x P^a_{fp} - F'_{pf} \partial_x X_5 = 0 \\
X_1 \partial_t X_6 + X_1 X_4 \partial_x X_6 + X_4 \partial_x P_p + p_p \partial_x X_4 + X_4 \alpha_p^\star \partial_x X_3 + X_4 F'_{pf} \partial_x X_5 = 0
\end{gathered} \tag{B 1}$$

with $\alpha_f = X_1 + X_2$, $\alpha_p^\star = 1 - X_2$, $\alpha_p = 1 - X_1 - X_2$, $p_p = X_1 \Theta_p (1 + 4\alpha_p^\star g_0)$,

$$P^a_{fp} = \frac{1}{\gamma_p} X_1 (X_4 - X_5)^2 (1 + 4\alpha_p^\star g_0),\ \Theta_p = (\gamma_p - 1)\left(X_6 - \frac{1}{2} X_4^2\right),\ g_0 = \frac{1 + \alpha_f}{2\alpha_f^3},$$

$P_p = p_p + P^a_{fp}$ and $F'_{pf} = (\gamma_p - 1)(1 - X_2)(X_5 - X_4)$. Note that P_p and P^a_{fp} depend on $(X_1, X_2, X_4, X_5, X_6)$. As discussed in Drew & Passman (1998), the incompressible model has two infinite and four finite eigenvalues.

The canonical form of (B 1) is

$$\mathbf{A}(\mathbf{X}) \partial_t \mathbf{X} + \mathbf{B}(\mathbf{X}) \partial_x \mathbf{X} = \mathbf{0} \tag{B 2}$$

with coefficient matrices

$$\mathbf{A} = \begin{bmatrix}
-1 & -1 & 0 & 0 & 0 & 0 \\
1 & 0 & 0 & 0 & 0 & 0 \\
0 & 1 & 0 & 0 & 0 & 0 \\
0 & 0 & 0 & X_1 & 0 & 0 \\
0 & 0 & 0 & 0 & X_2 & 0 \\
0 & 0 & 0 & 0 & 0 & X_1
\end{bmatrix} \tag{B 3}$$

and

$$\mathbf{B} = \begin{bmatrix}
-X_4 & -X_4 & 0 & 1 - X_1 - X_2 & 0 & 0 \\
X_4 & 0 & 0 & X_1 & 0 & 0 \\
0 & X_5 & 0 & 0 & X_2 & 0 \\
\frac{\partial P_p}{\partial X_1} & \frac{\partial P_p}{\partial X_2} & 1 - X_2 & X_1 X_4 + \frac{\partial P_p}{\partial X_4} & F'_{pf} + \frac{\partial P^a_{fp}}{\partial X_5} & \frac{\partial p_p}{\partial X_6} \\
-\frac{\partial P^a_{fp}}{\partial X_1} & -\frac{\partial P^a_{fp}}{\partial X_2} & X_2 & -\frac{\partial P^a_{fp}}{\partial X_4} & X_2 X_5 - F'_{pf} - \frac{\partial P^a_{fp}}{\partial X_5} & 0 \\
X_4 \frac{\partial P_p}{\partial X_1} & X_4 \frac{\partial P_p}{\partial X_2} & X_4 (1 - X_2) & p_p + X_4 \frac{\partial P_p}{\partial X_4} & X_4 (F'_{pf} + \frac{\partial P^a_{fp}}{\partial X_5}) & X_4 (X_1 + \frac{\partial p_p}{\partial X_6})
\end{bmatrix}. \tag{B 4}$$

The four finite eigenvalues, denoted by λ, for this system are found from the fourth-order characteristic polynomial defined by $|\mathbf{A}\lambda - \mathbf{B}| = 0$. If the roots of this polynomial are scaled as

$$\lambda^\star = \frac{\lambda - u_f}{u_p - u_f} \quad \text{and} \quad \Theta_r = \frac{\Theta_p}{(u_p - u_f)^2}, \tag{B 5}$$

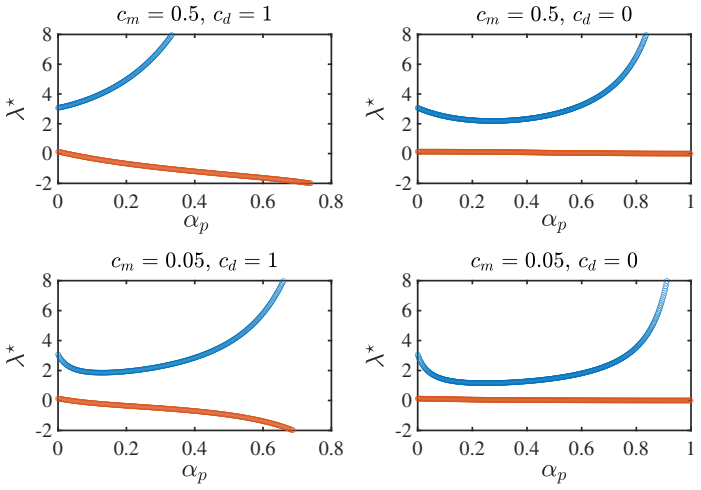

FIGURE 10. Eigenvalues of incompressible bubbly flow model versus α_p with $\alpha_a = c_m\alpha_f\alpha_p$, $\Theta_r = 2/\gamma_p^2$ and $\gamma_p = 5/3$. For $c_d = 1$ the eigenvalues are found with g_0, whereas for $c_d = 0$ the eigenvalues are found with $g_0 = 0$. Unlike in the compressible model, g_0 is not required to keep the system hyperbolic for large α_p. This "equilibrium" value for Θ_r results in one eigenvalue at zero when $g_0 = 0$, which corresponds to the fluid velocity. Conversely, the equilibrium value for Θ_r found from direct-numerical simulation could be used to specific γ_p for bubbly flow (i.e., $\gamma_p = 4.714$ using data from Tavanashad *et al.* 2019).

then two eigenvalues depend on c_m, α_p and Θ_r, and the other two are $\lambda^\star = 1$ (which corresponds to Ma_s in the main text). Examples of the α_p-dependence of the two non-constant eigenvalues are shown in figure 10. As noted in the main text when discussing (2.1), these eigenvalues do not represent the speed of sound in the fluid, which is infinite in this model.

For $\alpha_p = 0$, the two non-constant eigenvalues $\lambda^\star$ are

$$1 + \frac{1}{\gamma_p} \pm \sqrt{1 + \frac{1}{\gamma_p^2} + \gamma_p\Theta_r} \tag{B 6}$$

and, thus, do not depend on c_m (as is the case in (3.7) for $Z \to +\infty$). In (B 6), the γ_p contribution outside the radical comes from P^a_{fp}. As seen in figure 10, these two eigenvalues are real-valued for all α_p with $c_m = 1/2$, including with $g_0 = 0$. It is noteworthy that the particle-phase eigenvalues from (3.7) in the limit $Z \to +\infty$ are equal to (B 6). This would not be the case if the transport equation for E_p were replaced by an algebraic expression for Θ_p. In any case, it is remarkable that by adding a transport equation for the added mass *and* a model for the particle-pressure tensor that does not depend on granular temperature, the incompressible two-fluid model becomes globally hyperbolic.

Alternative forms for the particle-pressure tensor are also possible. For example, it is not necessary for $\alpha_a\boldsymbol{P}^a_{fp}$ to depend on g_0 or α_a. In figure 11, the eigenvalues for a fluid-mediated particle-pressure model that is quadratic in $\alpha_p^\star$:

$$P_p = p_p + c_f\gamma_p(\alpha_p^\star)^2\alpha_f^\star u_{fp}^2 \tag{B 7}$$

are plotted versus α_p. For $\alpha_p = 0$, the two non-constant eigenvalues with this particle-

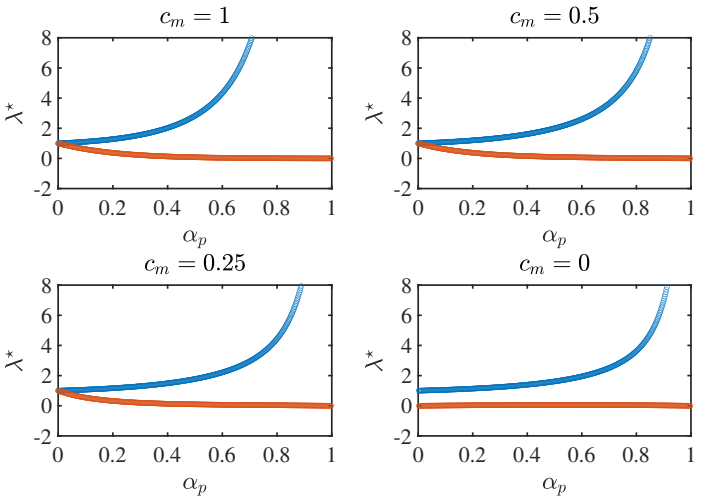

FIGURE 11. Eigenvalues of incompressible bubbly flow with an alternative fluid-mediated particle-pressure model versus α_p with $\alpha_a = c_m\alpha_f\alpha_p$, $\Theta_r = 0$ and $c_f\gamma_p = 5/30$. Here, the particle pressure is $P_p = p_p + c_f\gamma_p(\alpha_p^\star)^2\alpha_f^\star u_{fp}^2$ and the system is hyperbolic for $0.1 \leqslant c_f$ with $0 \leqslant c_m \leqslant 1$.

pressure model are

$$1 \pm \sqrt{\gamma_p\Theta_r}, \tag{B 8}$$

and they remain real-valued for all $\alpha_p \in [0, 1]$ if $0.1 \leqslant c_f$, independent of c_m. Comparing figures 10 and 11, we observe that with $0 < c_m$ the quadratic dependence on $\alpha_p^\star$ causes the two eigenvalues to be equal at $\alpha_p = 0$ when $\Theta_r = 0$. ($c_m = 0$ is a singular case where the lower eigenvalue jumps to zero as α_p increase from zero.) For $c_f < 0.1$, the eigenvalues are complex for small α_p, before becoming real-valued for larger volume fractions. Replacing $\alpha_p^\star$ by α_p in (B 7) gives qualitatively equivalent results, but the value of c_f must be slightly larger to ensure hyperbolicity. Although it introduces a new parameter c_f into the hyperbolicity analysis, the form of (B 7) is physically motivated by the fact that binary interactions between particles mediated by the fluid scale with α_p^2 in a dilute system. Also, note that the partial derivative of the second term in (B 7) with respect to $\alpha_p^\star$ has the form of the "turbulent-dispersion" force that is used to make bubbly-flow models hyperbolic (see, e.g., Panicker *et al.* 2018).

Finally, it is noteworthy that the partial derivatives of P_p appearing in the fourth row of $\mathbf{B}$ in (B 4) could be interpreted as arising due to separate forces. For example, $\partial P_p/\partial X_2$ might be attributed to "turbulent dispersion", while $\partial p_p/\partial X_6$ acts like a pseudo-turbulent turbophoresis. Nonetheless, they all have a common origin in the particle-phase pressure tensor.

REFERENCES

ABBAS, M., CLIMENT, E., PARMENTIER, J.-F. & SIMONIN, O. 2010 Flow of particles suspended in a sheared viscous fluid: Effects of finite inertia and inelastic collisions. *AIChE Journal* **56** (10), 2523–2538.

AUTON, T. R., HUNT, J. R. C. & PRUD'HOMME, M. 1988 The force exerted on a body in inviscid unsteady non-uniform rotational flow. *J. Fluid Mech.* **197**, 241–257.

BATCHELOR, G. K. 1988 A new theory of the instability of a uniform fluidized bed. *J. Fluid Mech.* **193**, 75–110.

Biesheuvel, A. & van Wijngaarden, L. 1984 Two-phase flow equations for a dilute dispersion of gas bubbles in liquid. *J. Fluid Mech.* **148**, 301–318.

Chalons, C., Fox, R. O., Laurent, F., Massot, M. & Vié, A. 2017 Multivariate Gaussian extended quadrature method of moments for turbulent fluid–particle flows. *Multiscale Modeling and Simulation* **15** (4), 1553–1583.

du Cluzeau, A., Bois, G. & Toutant, A. 2019 Analysis and modelling of Reynolds stresses in turbulent bubbly up-flows from direct numerical simulations. *J. Fluid Mech.* **866**, 132–168.

du Cluzeau, A., Bois, G., Toutant, A. & Martinez, J.-M. 2020 On bubble forces in turbulent channel flows from direct numerical simulations. *J. Fluid Mech.* **882**, A27.

Cook, T. L. & Harlow, F. H. 1984 Virtual mass in multiphase flow. *Int. J. Multiphase Flow* **10** (6), 691–969.

Drew, D., Cheng, L. & Lahey, R. T. 1979 The analysis of virtual mass effects in two-phase flow. *Int. J. Multiphase Flow* **5**, 233–242.

Drew, P. A. & Passman, S. L. 1998 *Theory of Multicomponent Fluids*. New York, USA: Springer.

Fox, R. O. 2019 A kinetic-based hyperbolic two-fluid model for binary hard-sphere mixtures. *J. Fluid Mech.* **877**, 282–329.

Gu, Y., Ozel, A., Kolehmainen, J. & Sundaresan, S. 2019 Computationally generated constitutive models for particle phase rheology in gas-fluidized suspensions. *J. Fluid Mech.* **860**, 318–349.

Guazzelli, É. & Pouliquen, O. 2018 Rheology of dense granular suspensions. *J. Fluid Mech.* **852**, P–1–73.

Hank, S., Saurel, R. & Le Metayer, O. 2011 A hyperbolic Eulerian model for dilute two-phase suspensions. *J. Modern Phys.* **2**, 997–1011.

Harlow, F. H. & Amsden, A. A. 1971 Fluid dynamics. *Tech. Rep.* LA-4700. Los Alamos National Laboratory.

Harten, A., Lax, P. D. & van Leer, B. 1983 On upstream differencing and Godunov-type schemes for hyperbolic conservation laws. *SIAM Rev.* **25** (1), 35–61.

Houim, R. W. & Oran, E. S. 2016 A multiphase model for compressible granular–gaseous flows: Formulation and initial tests. *J. Fluid Mech.* **789**, 166–220.

Kramer, O. J. I., de Moel, P. J., Baars, E. T., van Vugt, W. H., Padding, J. T. & van der Hoek, J. P. 2019 Improvement of the Richardson–Zaki liquid–solid fluidisation model on the basis of hydraulics. *Powder Technology* **343**, 465–478.

Kumbaro, A. & Ndjinga, M. 2011 Influence of interfacial pressure term on the hyperbolicity of a general multifluid model. *The Journal of Computational Multiphase Flows* **3** (3), 177–195.

Levermore, C. D. & Morokoff, W. J. 1996 The Gaussian moment closure for gas dynamics. *SIAM J. Appl. Math.* **59**, 72–96.

Lhuillier, D., Chang, C.-H. & Theofanous, T. G. 2013 On the quest for a hyperbolic effective-field model of disperse flows. *J. Fluid Mech.* **731**, 184–194.

Marchisio, D. L. & Fox, R. O. 2013 *Computational Models for Polydisperse Particulate and Multiphase Systems*. Cambridge, UK: Cambridge University Press.

Massoudi, M. 2002 On the importance of material frame-indifference and lift forces in multiphase flows. *Chem. Engng Sci.* **57**, 3687–3701.

Mei, R. & Adrian, R. J. 1992 Flow past a sphere with an oscillation in the free-stream velocity and unsteady drag at finite Reynolds number. *J. Fluid Mech.* **237**, 323–341.

Métivier, G. 2005 Remarks on the well-posedness of the nonlinear Cauchy problem. In *Contemp. Math., Geometric analysis of PDE and several complex variables*, vol. 368, pp. 337–356. Providence, RI: Amer. Math. Soc.

Milne-Thomson, L. M. 1968 *Theoretical Hydrodynamics*, 5th edn. New York, USA: Macmillan.

Moore, W. C. & Balachandar, S. 2019 Lagrangian investigation of pseudo-turbulence in multiphase flow using superposable wakes. *Physical Review Fluids* **4**, 114301.

Ndjinga, M. 2007 Influence of interfacial pressure on the hyperbolicity of the two-fluid model. *C. R. Acad. Sci. Paris 1* **344**, 407–412.

Odar, F. & Hamilton, W. S. 1964 Forces on a sphere accelerating in a vicous fluid. *J. Fluid Mech.* **18** (2), 302–314.

Osnes, A. N., Vartdal, M., Omang, M. G. & Reif, B. A. P. 2019 Computational analysis

of shock-induced flow through stationary particle clouds. *Int. J. Multiphase Flow* **114**, 268–286.

Osnes, A. N., Vartdal, M., Omang, M. G. & Reif, B. A. P. 2020 Particle-resolved simulations of shock-induced flow through particle clouds at different Reynolds numbers. *Physical Review Fluids* **5** (1), 014305.

Panicker, N., Passalacqua, A. & Fox, R. O. 2018 On the hyperbolicity of the two-fluid model for gas–liquid flows. *Appl. Math. Modelling* **57**, 432–447.

Peng, C., Kong, B., Zhou, J., Sun, B., Passalacqua, A., Subramaniam, S. & Fox, R. O. 2019 Implementation of pseudo-turbulence closures in an Eulerian–Eulerian two-fluid model for non-isothermal gas–solid flows. *Chem. Engng Sci.* **207**, 663–671.

Richardson, J. F. & Zaki, W. N. 1954 Sedimentation and fluidization: part I. *Trans. Inst. Chem. Eng.* **32**, 35–53.

Risso, F. 2018 Agitation, mixing, and transfers induced by bubbles. *Annu. Rev. Fluid Mech.* **50**, 25–48.

Sangani, A. S., Zhang, D. Z. & Prosperetti, A. 1991 The added mass, Basset, and viscous drag coefficients in nondilute bubbly liquids undergoing small-amplitude oscillatory motion. *Phys. Fluids A* **3**, 2955–2970.

Saurel, R. & Abgrall, R. 1999 A simple method for compressible multifluid flows. *SIAM J. Sci. Comput.* pp. 1115–1145.

Shallcross, G. S., Fox, R. O. & Capecelatro, J. 2020 A volume-filtered description of compressible particle-laden flows. *Int. J. Multiphase Flow* **122**, 103138.

Sturm, J. Ch. F. 1829 Mémoire sur la résolution des équations numériques. *Bulletin des Sciences de Férussac* **11**, 419–425.

Syamlal, M. 2011 A hyperbolic model for fluid–solids two-phase flow. *Chem. Engng Sci.* **66**, 4421–4425.

Tavanashad, V., Passalacqua, A., Fox, R. O. & Subramaniam, S. 2019 Effect of density ratio on velocity fluctuations in dispersed multiphase flow from simulations of finite-size particles. *Acta Mechanica* **230** (2), 469–484.

Tenneti, S., Garg, R. & Subramaniam, S. 2011 Drag law for monodisperse gas–solid systems using particle-resolved direct numerical simulation of flow past fixed assemblies of spheres. *Intl J. Multiphase Flow* **37** (9), 1072–1092.

Toro, E. F. 1997 *Riemann Solvers and Numerical Methods for Fluid Dynamics: A Practical Introduction*. Berlin, Germany: Springer.

Vazquez-Gonzalez, T., Llor, A. & Fochesato, C. 2016 Ransom test results from various two-fluid schemes: Is enforcing hyperbolicity a thermodynamically consistent option? *Intl J. Multiphase Flow* **81**, 104–112.

Vié, A., Doisneau, F. & Massot, M. 2015 On the anisotropic Gaussian velocity closure for inertial-particle laden flows. *Commun. Comput. Phys.* **17** (01), 1–46.

van Wijngaarden, L. 1976 Hydrodynamic interactions between gas bubbles in liquid. *J. Fluid Mech.* **77**, 27–44.

Zhang, D. Z. 2020 Stress from long-range interactions in particulate systems. *Tech. Rep.* LA-UR-20-23257. Los Alamos National Laboratory.

Zhang, D. Z., Ma, X. & Rauenzahn, R. M. 2006 Interspecies stress in momentum equations for dense binary particulate systems. *Physical Review Letters* **97**, 048301.

Zhang, D. Z. & Prosperetti, A. 1994 Averaged equations for inviscid dispersed two-phase flows. *J. Fluid Mech.* **267**, 185–219.

Zuber, N. 1964 On the dispersed two-phase flow in the laminar regime. *Chem. Engng Sci.* **19**, 897–917.